박 사 학 위 논 문

Isocitrate Dehydrogenase 2 Deficiency Induces Dysfunction of Energy Metabolism in Brown Adipose Tissue

계 명 대 학 교 대 학 원

의 학 과

이 재 호

지도교수 임 승 순

2 0 2 0 년 2 월

Isocitrate Dehydrogenase 2 Deficiency Induces Dysfunction of Energy Metabolism in Brown Adipose Tissue

지도교수 임 승 순

이 논문을 박사학위 논문으로 제출함

2020년 2월

계 명 대 학 교 대 학 원

의학과 생리학 전공

이 재 호

이재호의 박사학위 논문을 인준함

주 심 송 대 규

부 심 임 승 순

부 심 배 재 훈

부 심 권 택 규

부 심 우 창 훈

계 명 대 학 교 대 학 원

2 0 2 0 년 2 월

Acknowledgement

본 논문을 제출하기까지 정말 많은 시간이 들었고, 많은 이들의 도움을 받았습니다. 긴 시간 동안 항상 옆에서 연구의 방향을 제시해 주시고 부족한 부분들을 채워주신 지도 교수님 임승순 교수님과 심사위원을 맡아 주신 송대규 교수님, 배재훈 교수님, 권택규 교수님, 우창훈 교수님께 진심으로 감사드립니다.

저는 이곳에서 석사를 시작하고 지금까지 나이만 먹었지 부족한 점이 많았습니다. 하지만 함께 연구실에서 가족들보다 시간을 오래 보냈던 박사님들과 함께 학위를 거쳤던 분들 그리고 연구원분들의 도움과 조언이 있었기에 저의 부족함을 채우고 긴 시간을 버틸 수 있었습니다. 그 덕에 무사히 이 논문을 쓸 수 있었습니다.

그리고 언제나 집이 멀다고 시간이 없다고 자주 얼굴도 비추지 못하고 일년 동안 명절에나 겨우 맘 편하게 보던 아버지, 어머니, 누나 그리고 매형에게 정말 죄송스러운 마음뿐이었습니다. 이쪽 분야의 일에 대해 이해는 못하지만 그래도 반대하지 않고 꿋꿋하게 정신적인 버팀목이 되어 주었기에 많은 시간을 버틸 수 있었습니다.

그 외 언제나 저에게 많은 도움을 주신 분들께 감사드리고 이 논문을 바칩니다.

2020년 2월

이 재 호

Table of Contents

List of Tables

List of Figures

1. Introduction

Isocitrate dehydrogenase 2 (IDH2) is a nicotinamide adenine dinucleotide phosphate ($NADP^+$)-dependent enzyme located in the mitochondria and catalyzes the oxidative decarboxylation of isocitrate to alpha-ketoglutarate (αKG) in the tricarboxylic acid (TCA) cycle (1-3). Moreover, IDH2 participates in regulating mitochondrial oxidative stress by catalyzing the production of nicotinamide adenine dinucleotide hydrogen phosphate (NADPH) (4-6). Therefore, IDH2 acts as a critical factor in mitochondrial function as one of the metabolic enzymes that donates NADPH for redox balancing in multiple organs (7).

The role of IDH2 in cancer has been broadly studied and most studies included the induction of apoptosis by degradation of the cancer cell functions by loss of genes through gene mutation (8-13). Recent studies have suggested that IDH2 knockout (KO) mice could exacerbate mitochondrial dysfunction during the development of nonalcoholic steatohepatitis due to the enhanced accumulation of the mitochondrial reactive oxygen species (ROS) (14). However, the underlying molecular mechanism of the effect of IDH2 on metabolic diseases remains unclear.

Obesity is connected with several metabolic diseases including type 2 diabetes and cardiovascular disease (15-19). Mammalian adipose tissue has been traditionally divided into two different types (20,21). White adipose tissue (WAT) stores energy in unilocular adipocytes, whereas brown adipose tissue (BAT) dissipates energy through non-shivering thermogenesis in multi-locular adipocytes (22-24). Brown adipocytes generate heat and counteract obesity by virtue of abundant mitochondria and mitochondrial uncoupling protein 1 (UCP1) (25-27). Thus, there has been an emerging interest in brown fat as a potential target for

anti-obesity therapy.

BAT is the major organ for non-shivering thermogenesis in mammals (28). It presents a unique process for heat production in response to cold stress and provides a protective mechanism against obesity (29,30). Many features of the molecular mechanisms underlying the function of BAT are known; however, these studies do not comprehensively understand how BAT function is controlled and incorporated with the whole body metabolism to ensure efficient burning of the metabolic substrates for the provision of heat.

Heat generation in BAT is known to get induced to defend against obesity and insulin resistance in mice with high fat diet (HFD) (31). A potentially harmful drawback of the promoted uncoupled respiration is the generation of mitochondrial oxidative stress that must be restricted to inhibit the oxidative damage to enzyme complexes involved in the TCA cycle (32,33).

To modulate substrate flow and balance electron transfer, appropriate coordinated action of key mitochondrial electron transport (ET) enzymes is required (34). One of the key TCA steps includes the oxidative decarboxylation of isocitrate by IDH, leading to the production of αKG. IDH3 catalyzes the irreversible reaction between isocitrate and nicotinamide adenine dinucleotide (NAD^+) to form αKG. In contrast, IDH1 and IDH2 are marched with $NADP^+$ and NADPH, and exist in the cytosol and mitochondrial matrix. Mitochondrial NADPH is essential for the provision of dependent scavenging of mitochondrial ROS that occurs during the times of promoted ET chain activity (35,36).

Even though IDH2 has been supposed as a distinct enzyme in the regulation of mitochondrial ROS, its contribution to the mitochondrial function for energy metabolism such as obesity or thermogenesis remain unknown.

The study aimed to elucidate the physiologic mechanism by which IDH2 regulates energy metabolism, and to investigate the role of IDH2 on the regulation of HFD-induced obesity and cold-exposure in mice.

2. Materials and Methods

2.1. Animal Study:

Four-wk-old male IDH2 KO and WT mice with the C57BL/6J were used for this study. All mice were kept in SPF facility. These mice were fed either a low fat diet (LFD, 10% fat, Research Diet, New Brunswick, NJ, USA) or a HFD (60% fat, Research Diet, New Brunswick, NJ, USA)

Butylated hydroxyanisole (BHA, 7.5 g/kg, Sigma Aldrich, St. Louis, MO, USA) was co-treated as an anti-oxidant, when necessary. Body weight was checked weekly. Body composition was analyzed using nuclear magnetic resonance (NMR, LF50 body composition analysis-analyzer, Bruker, Brussels, Belgium). To analyze the thermogenesis function of BAT, control 8-wk-old mice were housed at 24 ℃ and cold-exposed groups were kept at 4 ℃ for 3 h. One percent αKG (Sigma Aldrich, St. Louis, MO, USA) was supplemented via drinking water for 4 wk. All procedures were carried out in accordance with the guidelines provided by Institution of Animal care and Use Committees KM-2015-32R3.

2.2. Materials:

Peroxisome proliferator-activated receptor gamma coactivator 1-alpha (PGC-1α), catalase (CAT), fibroblast growth factor 21 (FGF21), and total oxidative phosphorylation (OXPHOS) cocktail antibodies were purchased from Abcam (Cambridge, UK). The antibodies against sirtuin

1 (SIRT1), sirtuin 3 (SIRT3), acetylated-lysine, superoxide dismutase 2 (SOD2), peroxisome proliferator-activated receptor gamma (PPARγ), and UCP1 were purchased from Cell signaling (Beverly, MA, USA). Glutathione peroxidase 3 (GPX3) antibody was purchased from Adipogen (San Diego, CA, USA). Nicotinamide adenine dinucleotide synthetase 1 (NADSYN1) antibody was purchased from Aviva system biology (San Diego, CA, USA). Antibodies against nicotinamide phosphoribosyltransferase (NAMPT), 60 kDa heat shock protein (HSP60) and glyceraldehyde-3-phosphate dehydrogenase (GAPDH) were purchased from Santa Cruz (Dallas, TX, USA); the GAPDH antibody was used for loading control. BSA, Insulin, triiodothyronine (T3), rosiglitazone, and sodium palmitate were purchased from Sigma Aldrich (St. Louis, MO, USA).

2.3. Analysis of Metabolic Cages:

Mice were fed either LFD or HFD when relocated to single cages in Phenomaster system (TSE Systems Gmbh, Bad Homburg, Germany) for 3 days. During the analysis period, temperature, physical activity, food intake, drinking, oxygen and carbon dioxide contents, oxygen uptake (VO_2), and carbon dioxide production (VCO_2) were measured at the same time using standard indirect calorimetry analysis. Energy expenditure and respiratory exchange ratio were calculated automatically from VO_2 and VCO_2. The data were collected in TSE Phenomaster software (TSE Systems Gmbh, Bad Homburg, Germany).

2.4. Serum Profiling:

Trigryceride (TG), cholesterol, high-density lipoprotein (HDL), low-density lipoprotein (LDL), non-esterified fatty acids (NEFA), AST and ALT concentrations were measured by a Beckman Coulter AU480 automatic biochemistry analysis system (Model AU-480, Beckman Coulter, Krefeld, Germany).

2.5. Mice Positron Emission Tomography/Computed Tomography (PET/CT) Imaging:

For PET/CT imaging was performed with the Triumph II PET/CT system (LabPET8, Gamma Medica-Ideas, Waukesha, WI, USA). CT scans were recorded with an X-ray detector (fly acquisition, number of projections: 512, binning setting: 2, frame number: 1, X-ray tube voltage: 75 kVp, focal spot size: 50 μm, magnification factor: 1.5, matrix size: 512) immediately following the acquisition of PET images. The PET images were reconstructed using three-dimensional (3D)-OSEM iterative image reconstruction and CT images were reconstructed using filtered back-projections. Mice housed at ambient temperature (AT, 22−24 ℃) and fed the HFD for 4 wk were used for the study. All mice were anesthetized using 1−2% isoflurane gas during the imaging. PET images were co-registered with anatomical CT images using 3D image visualization and analysis software (VIVID, Gamma Medica-Ideas, Northridge, CA, USA).

2.6. Isolation of Primary Brown Adipocytes from BAT:

The primary brown adipocytes from 4-wk-old mice were separated by collagenase digestion. Briefly, the BAT are dissected, minced, and

digested with 0.2% type I collagenase (Worthington Biochemical Co., Freehold, NJ, USA) in DPBS buffer (Welgene, Daegu, Korea) for 40 min at 37 ℃. The brown adipocytes were separated from the cell pellet bycentrifugation at 1000 × *g* for 5 min at 4 ℃. The cell pellet was then suspended in fetal bovine serum (FBS, Hyclone, Logan, UT, USA) and filtered through a 40-μm mesh filter (BD Bioscience, San Diego, CA, USA). The pelleted primary brown adipocytes were re-suspended in Dulbecco's modified Eagle's medium (DMEM, Corning, NY, USA) containing 15% FBS and 1% penicillin/streptomycin, and subsequently seeded in six-well plates for proliferation. Cells were differentiated using a differentiation medium (DMEM containing 15% FBS, 50 nM insulin, 5 nM T3, and 1 μM rosiglitazone) for two days.

2.7. Mitochondrial ROS Production Assay:

Primary brown adipocytes (2×10^5 cells/well) were cultured in the absence or presence of 500 μM BSA-conjugated palmitate. Subsequently, 100 μM BHA was added to it and the cells were incubated for 1 h. MitoSOX™ Red mitochondrial superoxide indicator (MitoSOX Red, Molecular Probes, Eugene, OR, USA) was added to the cells and incubated at 37 ℃ for 15 min. The cells were harvested by treating with 0.05% trypsin-ethylenediaminetetraacetic acid and then washed twice with cold PBS. The cells conjugated with MitoSOX Red were detected using the fluorescence 1 setting of fluorescence-activated cell sorting (FACS) Calibur (BD Biosciences, San Diego, CA, USA).

2.8. Mitochondrial Oxygen Consumption Rate (OCR):

The mitochondrial OCR was measured with a Seahorse XF24 analyzer (Seahorse Bioscience Inc., North Billerica, MA, USA) in 24-well plates. Primary brown adipocytes were seeded at 2×10^4 cells per well before the analysis. On the day before the OCR measurement, the sensor cartridge was placed into calibration buffer (Seahorse Bioscience Inc., North Billerica, MA, USA) and incubated in a non-CO_2 incubator at 37 ℃. Primary brown adipocytes were washed and incubated in DMEM without sodium bicarbonate. The medium as well as mitochondrial OXPHOS inhibitors were adjusted to pH 7.4 on the day of the OCR assay. The basal OCR was measured three times and three readings were taken after the addition of each mitochondrial OXPHOS inhibitor [oligomycin (2 μg/mL) and rotenone (1 μM)]. The basal and post-oligomycin OCRs were calculated by averaging the last three measurements after the maintenance of a steady state. Coupled respiration was expressed as percent decrease from the basal respiration. Additionally, carbonyl cyanide 4-(trifluoromethoxy) phenylhydrazone (5 μM) was used to measure the maximal mitochondrial respiration of the cells. OCR was automatically calculated and recorded by the sensor cartridge and the Seahorse XF24 software.

2.9. Transmission Electron Microscopy (TEM):

The BAT samples from WT and IDH2 KO mice were prefixed in 2% paraformaldehyde and 2.5% glutaraldehyde (Electron Microscopy Sciences, Fort Washington, PA, USA) in 0.1 M phosphate buffer (pH 7.4). The tissues were removed and stored in the same fresh fixative overnight at 4 ℃. Tissues were washed, post-fixed in 1% osmium tetroxide for 2 h, dehydrated through an ascending series of ethanol,

propylene oxide and embedded in Epon mixture (Oken Shoji Co., Tokyo, Japan). Thin sections (70 nm) were made using Leica EM UC6 ultramicrotome (Leica Microsystems, Wetzlar, Germany), mounted on 200 mesh copper grids, stained with 2% uranyl acetate and 1% lead citrate for 5 min each, and observed under a Hitachi H-7650 transmission electron microscope (Hitachi, Tokyo, Japan) at the accelerating voltage of 80 kV.

2.10. RNA-sequencing (RNA-seq):

The BAT samples were collected from WT and IDH2 KO mice fed LFD or HFD. Same amounts of RNA from three individual mice were pooled together to make 3 separate samples for analysis by RNA-seq (Macrogen Inc., Seoul, Korea). Briefly, one μg of the total RNA was analyzed using the Truseq RNA library kit (Illumina, San Diego, CA, USA) to construct the cDNA libraries. The protocol included polyA-selected RNA extraction, RNA fragmentation, random hexamer primed reverse transcription, and 100 nt paired-end sequencing using an Illumina Hiseq 2000 (Illumina, San Diego, CA, USA). An agilent technologies' 2100 bioanalyzer was used for the qualification.

2.11. Quantitative Polymerase Chain Reaction (qPCR):

Total RNA was isolated using the TriZol reagent (Life Technologies, Carlsbad, CA, USA) and the cDNA was prepared using iScript cDNA synthesis kit (Bio-Rad, Hercules, CA, USA) according to the manufacturers' instructions. The qPCR was carried out using a CFX96^{TM} real time system (Bio-Rad, Hercules, CA, USA). The primer sequences

are listed in Table 1.

Threshold cycle (CT) number of each gene was calculated, and ribosomal protein L32 was used as reference genes. Delta-delta CT values of genes were presented as relative fold induction.

2.12. Westerm Blot Analysis:

Whole tissue lysate was extracted using RIPA lysis buffer [50 mM Tris-Hcl pH 8.0, 150 mM NaCl, 1.0% NP-40 or Triton X-100, 0.5% Na_3VO_4, and 0.1% sodium dodecyl sulfate (SDS)] containing complete protease inhibitor cocktail (GeneDepot, Barker, TX, USA). Proteins were diluted in loading dye, heated at 94 ℃ for 5 min. Lysates were centrifuged at 13,000 rpm for 15 min at 4 ℃ and the supernatant fractions were collected. Proteins were resolved by 5−10% Tris-HCl SDS/polyacrylamide gel electrophoresis gel electrophoresis and transferred onto nitrocellulose (GE-health care, Uppsala, Sweden). All immunoblots were developed by horseradish peroxidase-conjugated secondary antibody (Santa Cruz, Dallas, TX, USA) with an ECL detection system (Bio-Rad, Hercules, CA, USA).

2.13. Measurement of Mitochondrial DNA Copy Number:

Total DNA were extracted with the DNA isolation kit (Bioseum, Seoul, South Korea). For mitochondrial DNA (mtDNA) copy number measurement, qPCR was performed using a CFX96^{TM} Bio-Rad qPCR machine. utilizing cyclooxygenase-1 (COX1) primers for mtDNA and normalized against the nuclear H-19 gene. The relative mtDNA copy number was defined as the total amount of mtDNA divided by the total

amount of nuclear DNA.

2.14. Mitochondrial Protein Isolation:

To isolate mitochondrial protein, BAT tissues were processed for mitochondrial isolation using a mitochondria isolation kit (Thermo Scientific, Madison, WI, USA). Briefly, the tissues were disrupted by manual cutting and dounce homogenization. Samples were then incubated according to the manufacturer's protocol and centrifuged to isolate cytosolic and mitochondrial fractions. Mitochondrial fractions were washed and suspended in mitochondria lysis buffer and then subjected to Western blot analysis of total OXPHOS levels.

2.15. Extraction and LC/MS/MS Quantitation of Metabolites from Tissue Homogenates :

Frozen BAT from C57B/6J mice was homogenized in ice-cold 50% acetonitrile/50% water with 0.3% formic acid. Tissue homogenates were aliquoted for metabolomics assays and stored at -80 ℃. For the analysis of organic acids, homogenates (50 μL) were spiked with isotopically-labelled internal standards, extracted in ethylacetate, and organic acids in dried extracts were derivatized with O-benzylhydroxylamine using 1-ethyl-3-(3-dimethylaminopropyl)carbodiimide coupling chemistry according to prior studies (37). Then, derivatized organic acids were quantitated using multiple reaction monitoring on a Dionex UltiMate 3000 Quantiva triple quadrupole mass spectrometer (Thermo Scientific, Madison, WI, USA) as previously described.

For nicotinamide adenine dinucleotide hydrogen (NADH) and NADPH extraction, 100 μL aliquots of homogenates spiked with isotopically-labelled internal standards. This was followed by the addition of 100 μL of 1 M ammonium formate to adjust the pH to 4. Samples were vortexed thoroughly and centrifuged at 18,000 × *g* for 5 min at 10 ℃. The clarified homogenates were passed through an AcroPrep advance 3 K Omega filter plate (Pall Co., Ann Arbor, MI, USA) prior to LC/MS/MS analysis. Quantitation of reduced nucleotides was achieved using multiple reaction monitoring on a Dionex UltiMate 3000 HPLC Quantiva triple quadrupole mass spectrometer.

2.16. Statistical Analysis:

Data were analyzed using GraphPad Prism 5.0 for Windows (GraphPad Software Inc., San Diego, CA, USA). Student's t-test was two-tailed, and data are shown as mean ± SEM. P value less than 0.05 was considered significant; * $p < 0.05$, ** $p < 0.01$, *** $p < 0.001$.

Table 1. Primer List for qPCR

Name		Sequences (5'→3')
L32	sense	ACATTTGCCCTGAATGTGGT
	antisense	ATCCTCTTGCCCTGATCCTT
Pgc-1α	sense	AACAAGCACTTCGGTCATCCCTG
	antisense	TTACTGAAGTCGCCATCCCTTAG
Prdm16	sense	CAGCACGGTGAAGCCATTC
	antisense	GCGTGCATCCGCTTGTG
Ucp1	sense	GGATGGTGAACCCGACAACT
	antisense	AACTCCGGCTGAGAAGATCTTG
Cidea	sense	GCAGGAACTTATCAGCAAGA
	antisense	CGTAACCAGGCCAGTTGTGAT
Leptin	sense	ATTTCACACACGCAGTCGGTAT
	antisense	GGTGAAGCCCAGGAATGAAG
Adipoq	sense	GGCCGTTCTCTTCACCTACG
	antisense	TGGAGGAGCACAGAGCCAG
Errα	sense	CTCAGCTCTCTACCCAAACGC
	antisense	CCGCTTGGTGATCTCACACTC
Cpt1β	sense	GCACACCAGGCAGTAGCTTT
	antisense	CAGGAGTTGATTCCAGACAGGTA
Cox8b	sense	TGTGGGGATCTCAGCCATAGT
	antisense	AGTGGGCTAAGACCCATCCTG
Atp5b	sense	GGTTCATCCTGCCAGAGACTA
	antisense	AATCCCTCATCGAACTGGACG
Nampt	sense	GCAGAAGCCGAGTTCAACATC
	antisense	TTTTCACGGCATTCAAAGTAGGA
Nadsyn1	sense	ACGGCTGCTCACTACTTGTTA
	antisense	CTGAGAACCGAGGCAACTTC
Sod2	sense	GCACATTAACGCGCAGATCA
	antisense	AGCCTCCAGCAACTCTCCTT
Gpx3	sense	CCTTTTAAGCAGTATGCAGGCA
	antisense	CAAGCCAAATGGCCCAAGTT
Cat	sense	AATCCTACACCATGTCGGACA
	antisense	CGGTCTTGTAATGGAACTTGC
Sirt3	sense	ATCCCGGACTTCAGATCCCC
	antisense	CAACATGAAAAAGGGCTTGGG
Elovl3	sense	TCCGCGTTCTCATGTAGGTCT
	antisense	GGACCTGATCCAACCCTATGA
Fgf21	sense	GTACCTCTACACAGATGACGACCAA

	antisense	CGCCTACCACTGTTCCATCCT
Nrf2	sense	CTCGCTGGAAAAAGAAGTG
	antisense	CCGTCCAGGAGTTCAGAGG
Pparγ1	sense	TCGCTGATGCACTGCCTATG
	antisense	GAGAGGTCCACAGAGCTGATT
Cox7a1	sense	CAGCGTCATGGTCAGTCTGT
	antisense	AGAAAACCGTGTGGCAGAGA
Tfam	sense	ATTCCGAAGTGTTTTTCCAGCA
	antisense	TCTGAAAGTTTTGCATCTGGGT

Atp5b: ATP synthase F1 subunit beta; *Cat*: catase; *Cidea*: cell death-inducing DNA fragmentation factor alpha-like effector A; *Cox7a1*: cytochrome c oxidase subunit 7a1; *Cox8b*: cytochrome c oxidase subunit 8B; *Cpt1β*: carnitine palmitoyltransferase 1 beta; *Elovl3*: elongation of very long chain fatty acids protein 3; *Errα*: estrogen-related receptor alpha; *Fgf21*: fibroblast growth factor 21; *Gpx3*: glutathione peroxidase 3; *L32*: ribosomal protein L32; *Nadsyn1*: nicotinamide adenine dinucleotide synthetase 1; *Nampt*: nicotinamide phosphoribosyltransferase; *Nrf2*: nuclear factor erythroid 2-related factor 2; *Pgc-1α*: Peroxisome proliferator-activated receptor gamma coactivator 1-alpha; *Pparγ1*: peroxisome proliferator-activated receptor gamma 1; *Prdm16*: positive regulatory domain containing 16; Sirt3: sirtuin 3; *Sod2*: superoxide dismutase 2; *Tfam*: transcription factor A, mitochondrial; *Ucp1*: mitochondrial uncoupling protein 1.

3. Results

3.1. IDH2 Protects from HFD-induced Metabolic Stress in BAT Mitochondria:

3.1.1. IDH2 KO Mice Are More Responsive toward HFD-induced Obesity:

To examine the effects of IDH2 on whole body energy homeostasis during metabolic stress, this data compared body weight gain in WT and IDH2 KO mice fed a HFD or LFD (Figure 1A). As a result, it was supported that HFD-IDH2 KO mice gained more weight and showed an increase in the amount of white fat (Figure 1B-D). The IDH2 KO mice on HFD started to gain body weight more quickly of doubled by 4 wk despite having eaten the same amount of diet (Figure 2A&B). Most of the excessive body weight in the HFD-IDH2 KO mice was because of a rise in fat mass and a decline in lean mass (Figure 2C&D). There was a significant increase in the serum level of ALT in serum of IDH2 KO (Figure 3A-G). In agreement with the increased body weight, there was a significant impairment in the whole-body energy expenditure in HFD-IDH2 KO mice (Figure 4A&B). There were no differences observed for physical activity, food intake or water consumption (Figure 5A-D). These results indicate that IDH2 KO mice drastically increases the fat accumulation during HFD, which can, in part, be attributed to a reduction in the whole body energy expenditure.

3.1.2. HFD Impairs BAT Function in IDH2 KO Mice:

IDH2 was expressed at high levels in the heart, kidney, muscle, and

BAT as was revealed by the tissue survey (Figure 6). Previous study has shown that IDH2 KO mice were susceptible to increased heart failure with mitochondrial dysfunction (38). Another recent report has shown that IDH2 KO mice had an increased frequency of hepatic steatosis than WT fed a HFD (14). Thus, this study hypothesized that IDH2 might defend against HFD-induced body weight gain and the associated metabolic disease. Consistent with this hypothesis, BAT depots of HFD-IDH2 KO mice were expanded and pale, suggesting a decrease in BAT energy expenditure (Figure 7A). Consistent with the expression of BAT-related genes such as *Pgc-1α*, positive regulatory domain containing 16 (*Prdm16*), *Ucp1* and cell death-inducing DNA fragmentation factor alpha-like effector A (*Cidea*) decreased (Figure 7B) and the expression of WAT-related genes such as *Leptin* and *Adipoq* increased in BAT of HFD-IDH2 KO mice (Figure 7C). These results provided further evidence supporting the hypothesis that BAT function is significantly impaired in HFD-IDH2 KO mice.

3.1.3. BAT Impairment in IDH2 KO Is Caused by Mitochondrial Dysfunction:

IDH2 is a mitochondrial enzyme required for maintaining the redox balance. Therefore, this study hypothesized that excessive body weight gain in HFD-IDH2 KO mice might result from mitochondrial dysfunction. Gene expression profiles by an RNA-seq analysis for BAT in WT and IDH2 KO mice confirmed that many genes expressed at lower levels in IDH2 KO mice were linked with mitochondrial function. These included genes that were down-regulated only in HFD-IDH2 KO BAT or those expressed at lower levels in BAT of IDH2 KO mice fed both LFD and HFD (Figure 8A). The decreased gene expression in IDH2 KO BAT is, at least, partly due to the reduced activity of

PGC-1α protein in IDH2 KO BAT (Figure 8B-D). In addition, expression of the estrogen-related receptor alpha (*Errα*) was also found to have reduced in IDH2 KO BAT (Figure 9A) along with that of several other known *Errα* and *Pgc-1α* target genes analyzed directly by qPCR (Figure 9A). The levels of mitochondrial DNA were also lower in BAT from IDH2 KO mice (Figure 9B). Further, the TEM images showed weak mitochondrial structure with disrupted cristae in BAT from the HFD-IDH2 KO mice (Figure 9C). A direct analysis of mitochondrial respiration using the Seahorse also showed that the IDH2 KO BAT underwent a dramatic reduction in the total OCR (Figure 9D).

This study checked the levels of TCA cycle intermediates and nicotinamide, these data observed that following IDH, TCA intermediates as well as NAD^+, NADH, $NADP^+$, and NADPH were significantly lower in BAT of HFD-IDH2 KO mice (Figure 10A-C). The RNA-seq data also suggested that the expression of *Nampt* and *Nadsyn1* was reduced in BAT of HFD-IDH2 KO mice. These two enzymes are involved in the production of NAD^+ through the kynurenine and salvage pathways, respectively. Direct qPCR for *Nampt* and *Nadsyn1* mRNA and Western blot data for NAMPT protein confirmed that their levels were reduced in IDH2 KO BAT (Figure 11A-C).

Decreased levels of NAMPT and NADSYN1 protein were consistent with the lower levels of nicotinamide. In addition, NAD^+ is an allosteric regulator of the sirtuin family of deacetylases. In fact, PGC-1α and SOD2 are directly deacetylated by SIRT1 and SIRT3, respectively, (39,40) and, both PGC-1α and SOD2 are known to play important roles in the mitochondrial function. In concordance with these previous studies, expression of SIRT1 and SIRT3 was lower in BAT from IDH2 KO mice both LFD and HFD (Figure 11D). The protein acetylation levels were also significantly higher in the IDH2 KO BAT (Figure 11E).

3.1.4. Ablation of IDH2 Leads to Up-regulated Accumulation of ROS:

To directly calculate the ROS levels, brown adipocytes isolated from BAT of WT and IDH2 KO mice were treated with the MitoSOX Red dye. The FACS analysis data revealed significantly higher levels of MitoSOX Red staining in BAT from IDH2 KO mice. This alteration was sustained when the cells were treated with BSA-conjugated palmitate to increase the ROS production (Figure 12A&B). Levels of mRNA and protein for CAT, SOD2, and GPX3, which are mitochondrial anti-oxidants genes, were also found to have decreased in BAT from the IDH2 KO mice on both LFD and HFD (Figure 13A&B). Taken together, these data suggest that ablation of IDH2 results in the dysfunction of ROS regulation when the mice were exposed to HFD, they could not control the excessive ROS accumulation, resulting in oxidative damage to mitochondria.

3.1.5. Supplementation of an Anti-oxidant Restores the Energy Imbalance and Obesity in HFD-IDH2 KO Mice:

This study hypothesized that the inhibition of ROS accumulation would restore the mitochondrial dysfunction and weight gain phenotype in the HFD-IDH2 KO mice. To test this, this study supplemented the bioavailable anti-oxidant BHA (41) to the LFD and HFD for WT and IDH2 KO mice. Interestingly, BHA supplementation significantly decreased the body weight gain in both WT and IDH2 KO mice despite having eaten the same amount of diet (Figure 14A&B). The decline in the weight gain was in accordance with a decrease in total fat mass (Figure 14C). Lean body mass was also normalized by BHA supplementation in WT and IDH2 KO mice (Figure 14D). BHA

treatment also decreased the levels of MitoSOX Red staining in brown adipocytes treated with BSA-conjugated palmitate (Figure 15A&B) while increasing both the energy expenditure and mitochondrial DNA copy number in HFD-IDH2 KO BAT (Figure 15C&D).

To verify gene expression that might help define the BHA-mediated protection from HFD-induced weight gain, this study performed RNA-seq in BAT from WT and IDH2 KO mice with HFD or HFD supplemented with BHA. It was observed that the levels of 1396 genes were decreased by 1.5-fold or more due to the HFD in IDH2 KO BAT relative to that in WT BAT (Figure 16A&B). Further, expression of 24 genes among them was significantly increased by BHA treatment (Figure 16C). These included genes that contribute to the mitochondrial function, energy expenditure, NAD regulation, and ROS resolution such as *Pgc-1α*, *Ucp1*, *Sirt3*, *Gpx3*, *Sod2*, *Cat*, and *Nampt* as well as *Nadsyn1* (Figure 17A-H). Protein levels for these genes showed partial restoration with BHA treatment (Figure 18A). The increases in acetyl-lysine of global protein levels were also changed by the BHA treatment (Figure 18B). Taken together, these results indicate that the BHA-mediated ROS scavenging results in, at least, a partial recovery of mitochondrial function and body weight gain, suggesting that the major reason behind the excessive weight gain and mitochondrial dysfunction could be increased downstream ROS resulting from the ablation of IDH2.

3.2. IDH2 Deficiency Induces Dysfunction of Brown Adipose Tissue in Acute Thermogenic Effects:

3.2.1. IDH2 Deficiency Leads to Impaired Thermogenesis in Mice

under the Cold Environment:

To evaluate cold-induced non-shivering thermogenesis in IDH2 KO mice, they were exposed to 4 ℃ for 3 h and then compared to the animals maintained at AT. Both WT and IDH2 KO mice had a similar rectal temperature under the AT and at the early time points (within 1 h) after the cold challenge at 4 ℃ (Figure 19A&B). However, IDH2 KO mice showed a significantly lower rectal temperature than WT mice after exposure to cold for 3 h (Figure 19B), suggesting that IDH2 was required for maintaining the whole-body temperature by non-shivering thermogenesis. Consistent with this model, visual inspection showed that the BAT depots of IDH2 KO mice after cold exposure were bleached, suggesting a decrease in BAT energy expenditure (Figure 19B). Taken together, these results indicated that IDH2-deficiency caused increased BAT-whitening and induced thermogenic dysfunction.

3.2.2. IDH2 Ablation Decreases Thermogenesis and Mitochondrial Biogenesis Marker Genes in BAT:

The BAT from cold-exposed IDH2 KO mice tended to have markedly lower mRNA levels of thermogenic genes such as *Ucp1*, *Cidea*, *Prdm16*, elongation of very long chain fatty acids protein 3 (*Elovl3*), and *Fgf21* than those of WT after cold challenge (Figure 20A). These results suggested that IDH2 genetic ablation decreased the thermogenic effects of BAT under cold stimulation. The test mice also showed reduced expression of mitochondrial biogenesis genes such as *Pgc-1α*, peroxisome proliferator-activated receptor gamma 1 (*Pparγ1*), nuclear factor erythroid 2-related factor 2 (*Nrf2*), cytochrome c oxidase subunit 8B (*Cox8b*), cytochrome c oxidase subunit 7a1 (*Cox7a1*), ATP synthase F1 subunit beta (*Atp5b*) and transcription factor A mitochondrial (*Tfam*) (Figure 20B). Protein levels for UCP1, FGF21, PGC-1α, and PPARγ

were decreased in IDH2 KO BAT (Figure 20C). This evident decreased in IDH2 KO BAT was underscored by decreased amounts of proteins belonging to complexes I−V in mitochondria (Figure 21). These findings suggest that IDH2 deficiency in BAT protects the mice from obesity and the related complications by elevating the energy expenditure.

3.2.3. Supplementation of Alpha-ketoglutarate Recovers Thermogenic Impairment in Cold-exposed IDH2 KO Mice:

The levels of metabolic intermediates of TCA cycle, such as succinate, fumarate, malate, and citrate which are down stream products of αKG were found to have been significantly reduced in IDH2 KO BAT (Figure 10C). Therefore, this study hypothesized that the supplementation of αKG might recover the thermogenic impairment in cold-exposed IDH2 KO mice. To test the effect of αKG on BAT, WT and IDH2 KO mice were exposed to 1% αKG via drinking water for 4 wk. Interestingly, αKG supplementation dramatically recovered the body temperature upon cold exposure in IDH2 KO mice (Figure 22A). Unlike in control IDH2 KO BAT, BAT of αKG-treated IDH2 KO mice exhibited mild changes with a browning process upon cold exposure (Figure 22B). At the mRNA level, the expression of thermogenic genes (*Ucp1*, *Cidea*, *Elovl3*, and *Fgf21*) (Figure 23A-D) and mitochondrial biogenesis genes (*Pgc-1α*, *Nrf2*, *Pparγ1*, *Cox7a1*, and *Tfam*) (Figure 23E-I) was found to be higher in BAT of the αKG-treated IDH2 KO mice than that in the control IDH2 KO mice. These results suggest that αKG stimulation enhances the thermogenesis of BAT through upregulation of the thermogenesis and mitochondrial biogenesis genes in the IDH2 deficient BAT depots, thus, leading to increased energy expenditure.

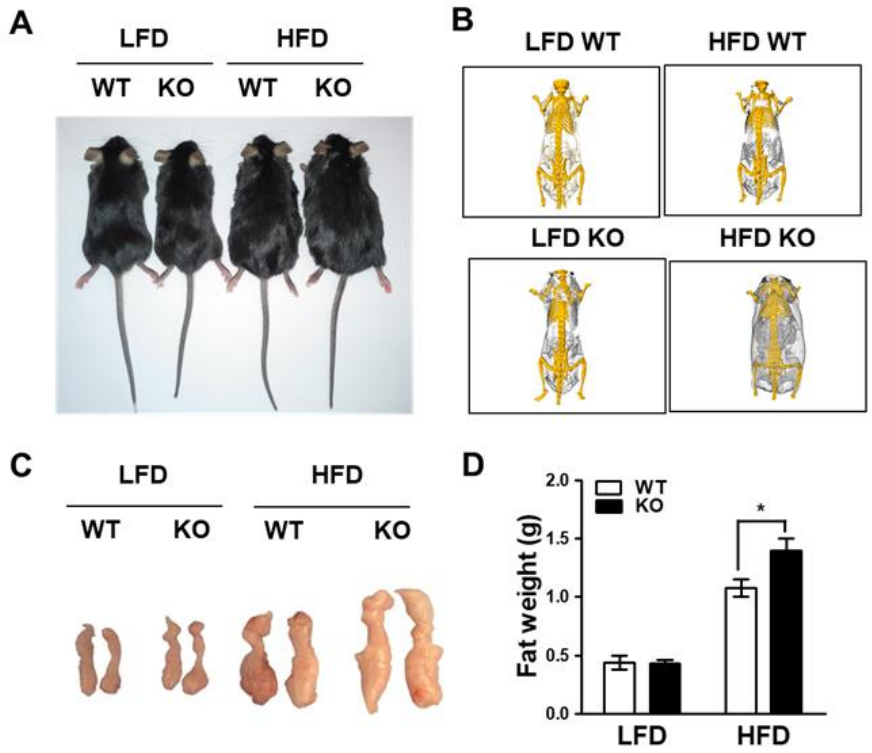

Figure 1. Increased fat accumulation by HFD in IDH2 KO mice. (A) Representative photograph of WT and IDH2 KO mice after 4 wk of HFD feeding. (B) CT images of mice on LFD and HFD after the 4 wk. (C) Images of gonadal fat depot. (D) Relative fat weight of WT and IDH2KO mice. * $p < 0.05$ vs. HFD WT. HFD: high fat diet; IDH2: isocitrate dehydrogenase 2; KO: knockout; LFD: low fat diet; WT: wild type.

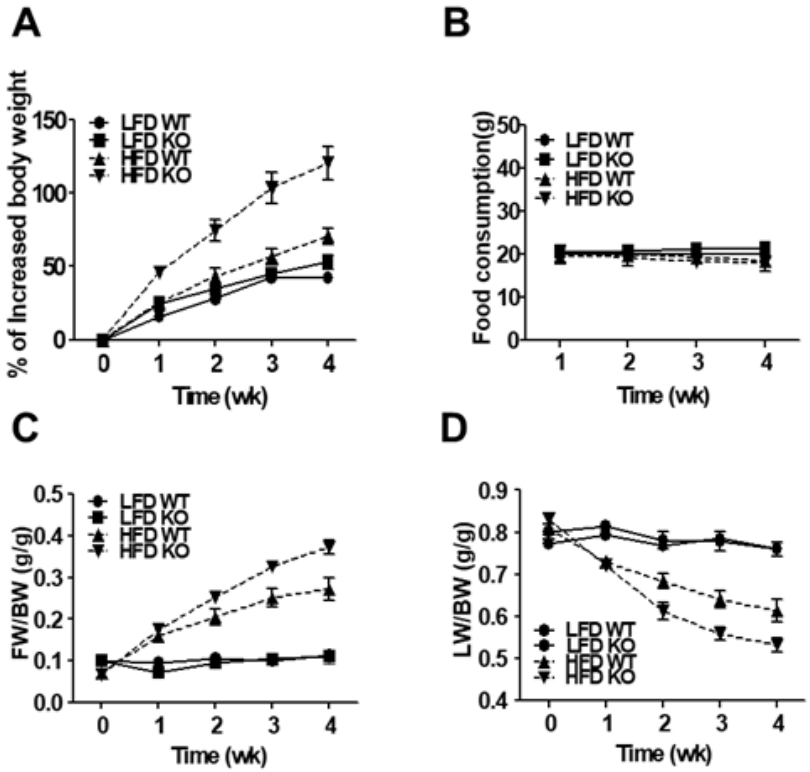

Figure 2. HFD leads to change of body composition in IDH2 KO mice. (A&B) Increased body weight and food consumption in each group over a period of 4 wk. (C&D) Time course of change in fat mass and lean body mass by NMR based on body composition. BW: body weight; FW: fat mass; LW: lean mass; NMR: nuclear magnetic resonance.

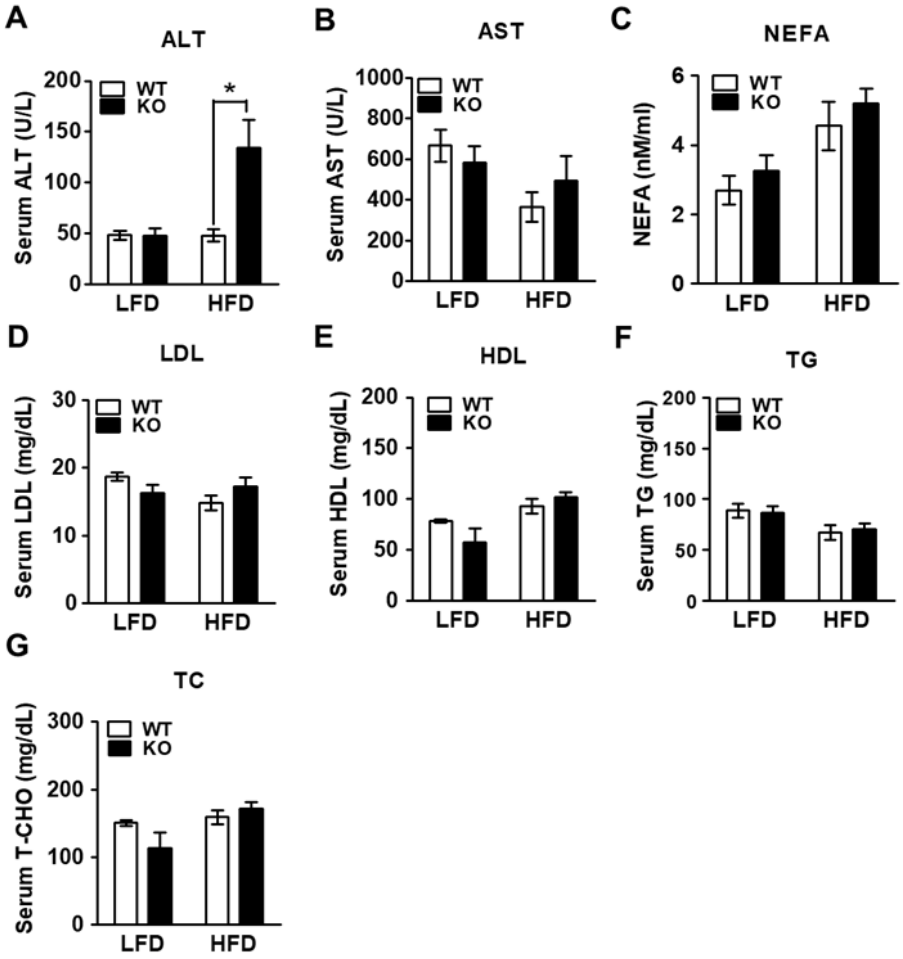

Figure 3. Serum profiling analysis. Serum lipid and liver toxicity marker profiling analysis of WT and IDH2 KO mice after 4-wk LFD and HFD. * $p < 0.05$ vs. HFD WT. HDL: high-density lipoprotein; LDL: low-density lipoprotein; NEFA: non-esterified fatty acids; TC: total cholesterol; TG: triglyceride.

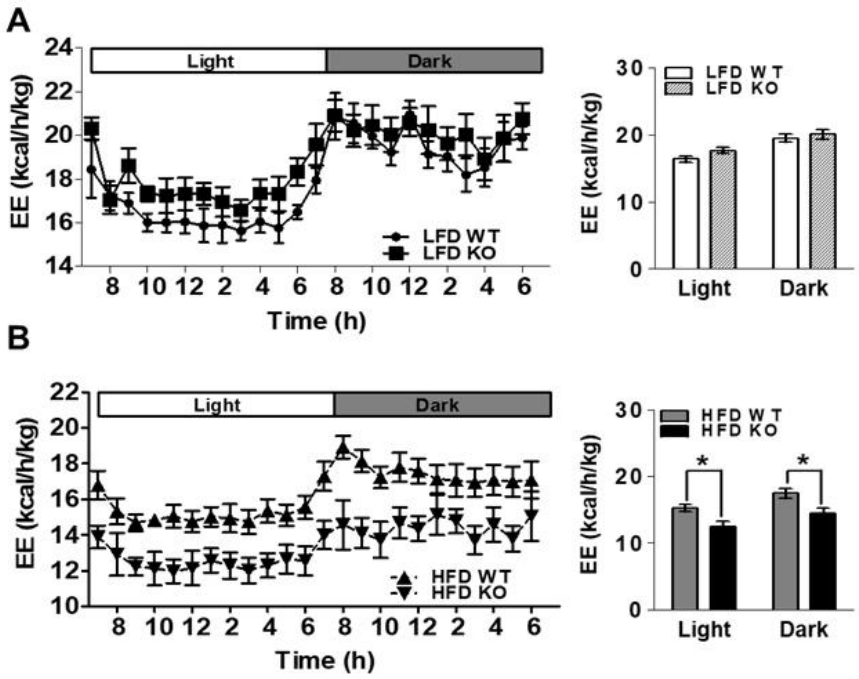

Figure 4. Lower energy expenditure in IDH2 KO mice. Energy expenditure over 24 h period was measured. (A&B) WT and IDH2 KO mice fed with LFD and HFD for 4 wk. * $p < 0.05$, vs. HFD WT. EE: energy expenditure.

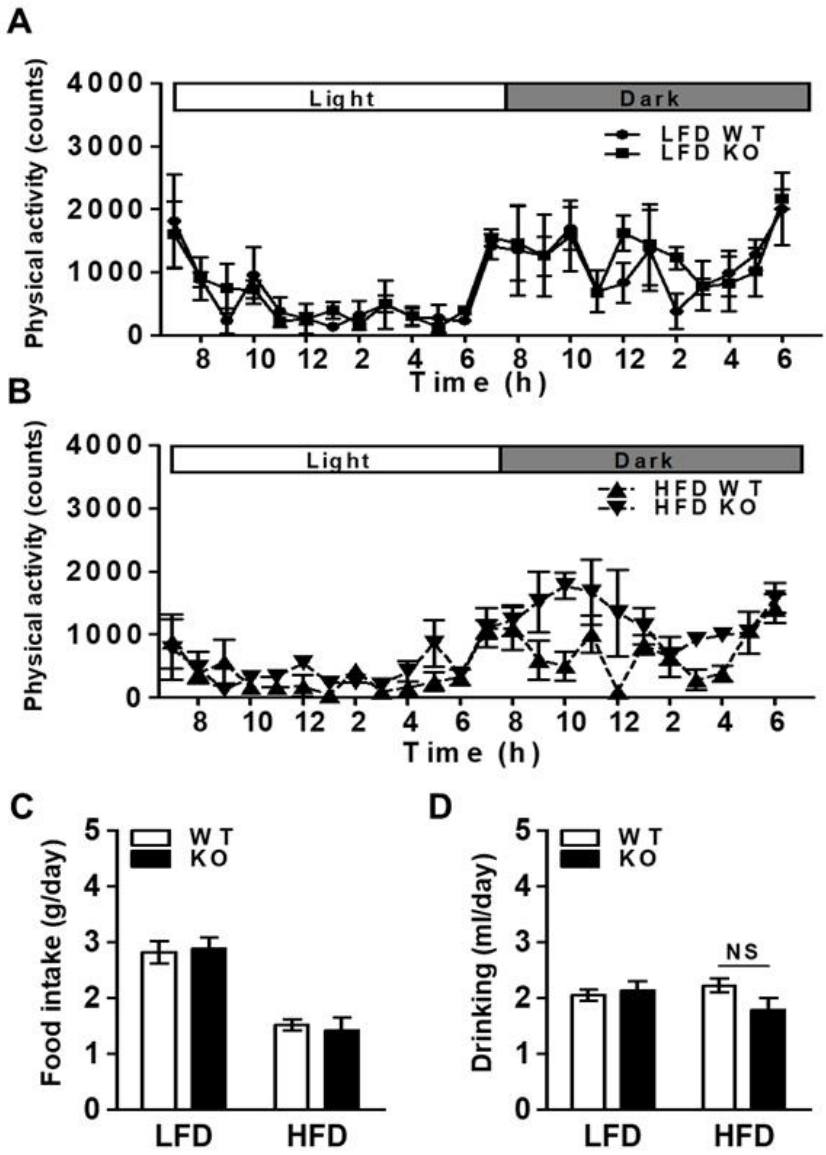

Figure 5. Lower physical activity of the IDH2 KO mice. (A&B) Physical activity during 24 h light and dark cycles recorded at the second day after 1-day acclimatization in WT and IDH2 KO mice fed with LFD and HFD for 4 wk. (C&D) Average amount of food and water intake over a 24 h. NS: not significant.

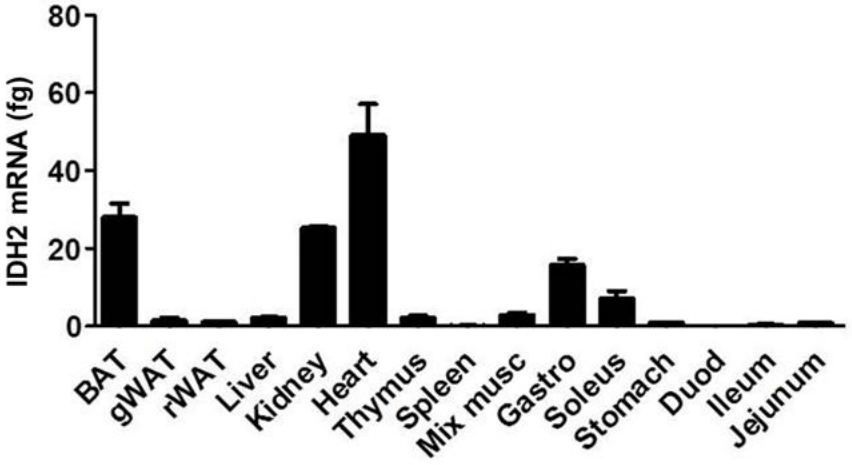

Figure 6. Tissue survey of IDH2 gene expression level. Total RNA from the individual tissues was used for qPCR with an internal control DNA standard for quantitation. Values are presented as femtogram of RNA/mg total RNA. Data are from pooled RNA samples from WT mice. BAT: brown adipose tissue; Duod: duodenum; fg: femto gram; Gastro: gastrocnemius muscle; gWAT: gonadal white adipose tissue; IDH2: isocitrate dehydrogenase 2; Mix musc: mixed muscle; rWAT: retroperitoneal white adipose tissue.

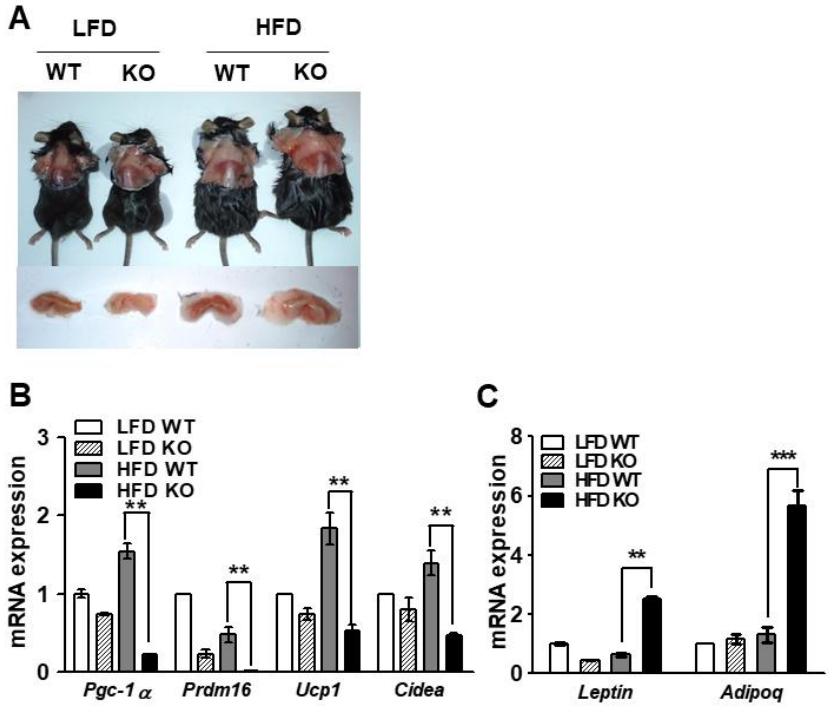

Figure 7. IDH2 deficiency induces BAT whitening. (A) Representative image showing BAT deposits. (B) Expression levels of BAT marker genes (*Pgc-1α*, *Prdm16*, *Ucp1*, and *Cidea*) in BAT were assessed by qPCR. (C) mRNA levels of WAT related genes (*Leptin* and *Adipoq*) in BAT. Total mRNAs were collected and analyzed by qPCR with indicated primers. ** $p < 0.01$ and *** $p < 0.001$ vs. HFD WT. *Cidea*: cell death-inducing DNA fragmentation factor alpha-like effector A; *Pgc-1α*: peroxisome proliferator-activated receptor gamma coactivator 1-alpha; *Prdm16*: positive regulatory domain containing 16; *Ucp1*: mitochondrial uncoupling protein 1.

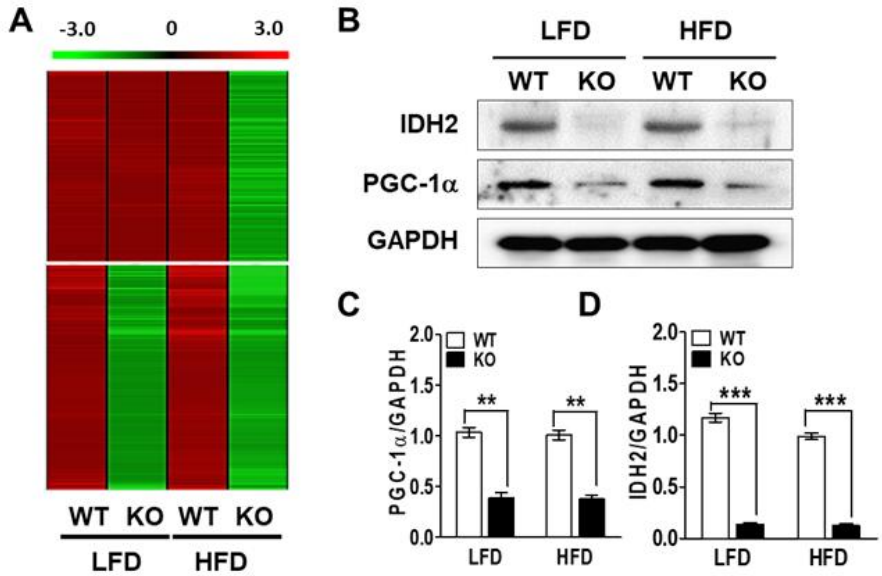

Figure 8. Ablation of IDH2 reduces expression of mitochondria-related genes in BAT. (A) Heat map representation of down regulated genes in IDH2 KO BAT of HFD sample (top) or down regulated in both LFD and HFD (bottom). (B) Western blot data of IDH2 and PGC-1α from BAT of WT and IDH2 KO mice when placed on LFD and HFD. GAPDH was used as a loading control. (C&D) Quantification of IDH2 and PGC-1α protein level. ** $p < 0.01$ and *** $p < 0.001$ vs. WT. GAPDH: glyceraldehyde-3-phosphate dehydrogenase.

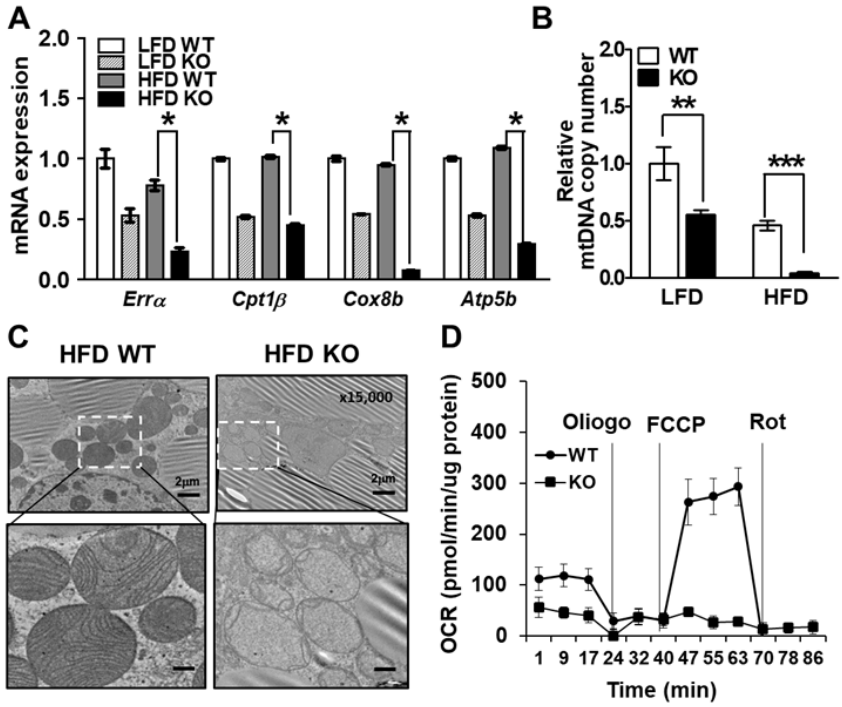

Figure 9. Deficiency of IDH2 decreases mitochondrial function in BAT. (A) Mitochondrial biogenesis-related genes expression in BAT at WT and IDH2 KO mice. (B) Relative mtDNA content expressed as a function of total nDNA in WT and IDH2 KO BAT. (C) TEM showed multiple sphere-shaped mitochondria, which is characteristic of BAT. (D) Representative time course of OCR of primary brown adipocytes from BAT of WT and IDH2 KO mice. * $p < 0.05$, ** $p < 0.01$ and *** $p < 0.001$ vs HFD WT or LFD WT. *Atp5b*: ATP synthase F1 subunit beta; Cox8b: cytochrome c oxidase subunit 8B; *Cpt1β*: carnitine palmitoyltransferase 1 beta; *Errα*: estrogen-related receptor alpha; FCCP: carbonyl cyanide 4-(trifluoromethoxy) phenylhydrazone; mtDNA: mitochondrial DNA; nDNA: nuclear DNA; OCR: oxigen consumption rate; Oligo: oligomicin; Rot: rotenone.

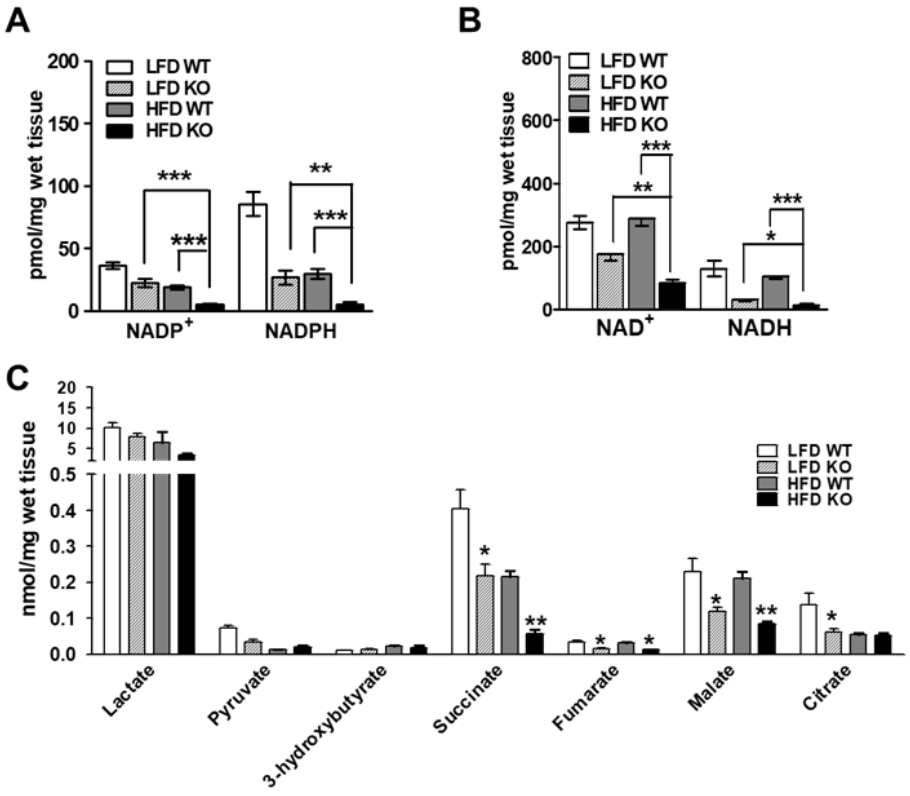

Figure 10. Organic acid levels from metabolomics analysis. LC/MS/MS analysis was used to measure metabolites associated with mitochondrial function. (A&B) The quantification of NAD^+ and NADH, $NADP^+$ and NADPH were determined in BAT of WT and IDH2 KO mice. (C) The level of organic acids was measured in WT and IDH2 KO BAT. * $p < 0.05$ vs and ** $p < 0.01$ vs LFD WT or HFD WT. * $p < 0.05$. NAD^+: nicotinamide adenine dinucleotide; NADH: nicotinamide adenine dinucleotide hydrogen; $NADP^+$: nicotinamide adenine dinucleotide phosphate; NADPH: nicotinamide adenine dinucleotide hydrogen phosphate.

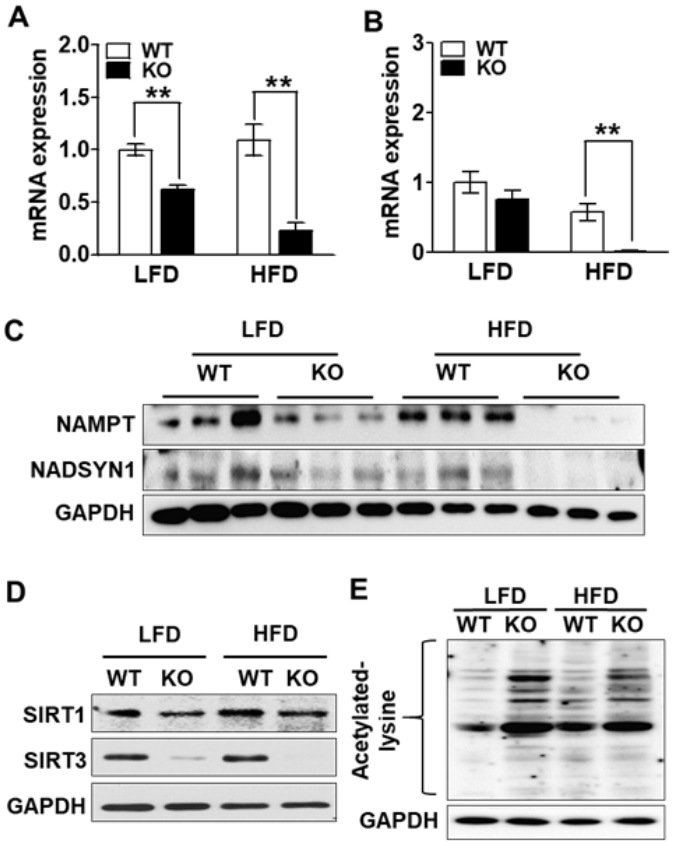

Figure 11. Nicotinamide levels are decreased in BAT of IDH2 KO mice. (A&B) mRNA expression levels of *Nampt* and *Nadsyn1* in BAT from WT and IDH2 KO mice. (C) Western blot data of NAMPT and NADSYN1 from BAT of WT and IDH2 KO mice when placed on LFD and HFD. (D) Protein levels for SIRT1 and SIRT3 in BAT from WT and IDH2 KO mice. (E) Acetylated-lysine level of whole protein in BAT of LFD and HFD WT and IDH2 KO mice. * $p < 0.05$, ** $p < 0.01$ and *** $p < 0.001$ vs. LFD WT, LFD KO or HFD WT. *Nadsyn1*: nicotinamide adenine dinucleotide synthetase 1; *Nampt*: nicotinamide phosphoribosyltransferase; SIRT1: sirtuin 1; SIRT3: sirtuin 3.

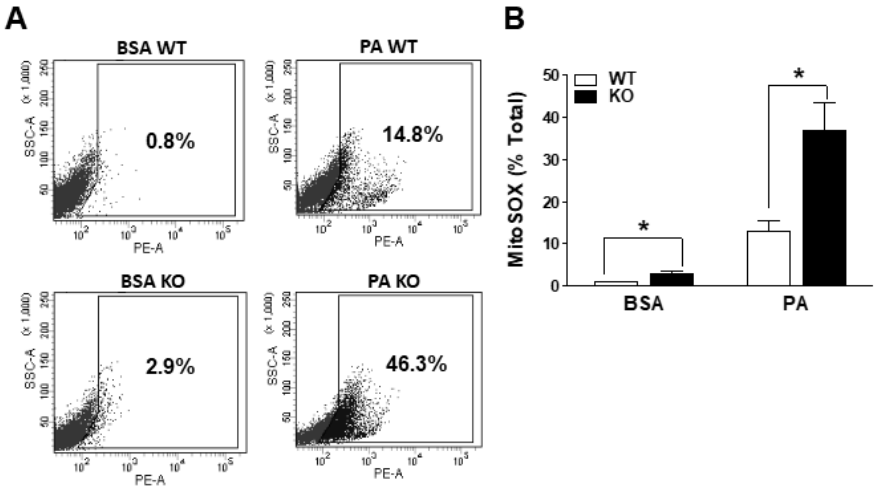

Figure 12. ROS production in brown adipocytes of the WT and IDH2 KO mice. (A) Primary brown adipocytes were cultured from WT and IDH2 KO mice and treated with BSA or BSA-conjugated palmitate and stained with MitoSOX-Red followed by FACS analysis. (B) Quantification of FACS data. * $p < 0.05$, vs. BSA WT or PA WT. FACS: fluorescence-activated cell sorting; mitoSOX: mitochondrial superoxide; PA: palmitic acid; PE: phycoerythrin; ROS: reactive oxygen species; SSC: side scatter.

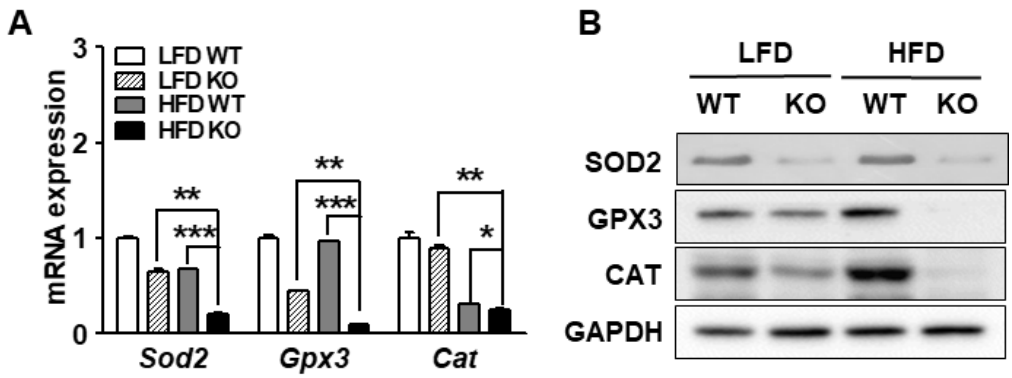

Figure 13. The effects of ROS production in the WT and IDH2 KO BAT. (A) mRNA levels of anti-oxidant genes (*Sod2*, *Gpx3*, *Cat*) in BAT of WT and IDH2 KO mice. (B) Western blot analysis of BAT from WT and IDH2 KO mice for the anti-oxidant genes. * $p < 0.05$, ** $p < 0.01$ and *** $p < 0.001$ vs. LFD KO or HFD WT. *Cat*: catase; *Gpx3*: glutathione peroxidase 3; *Sod2*: superoxide dismutase 2.

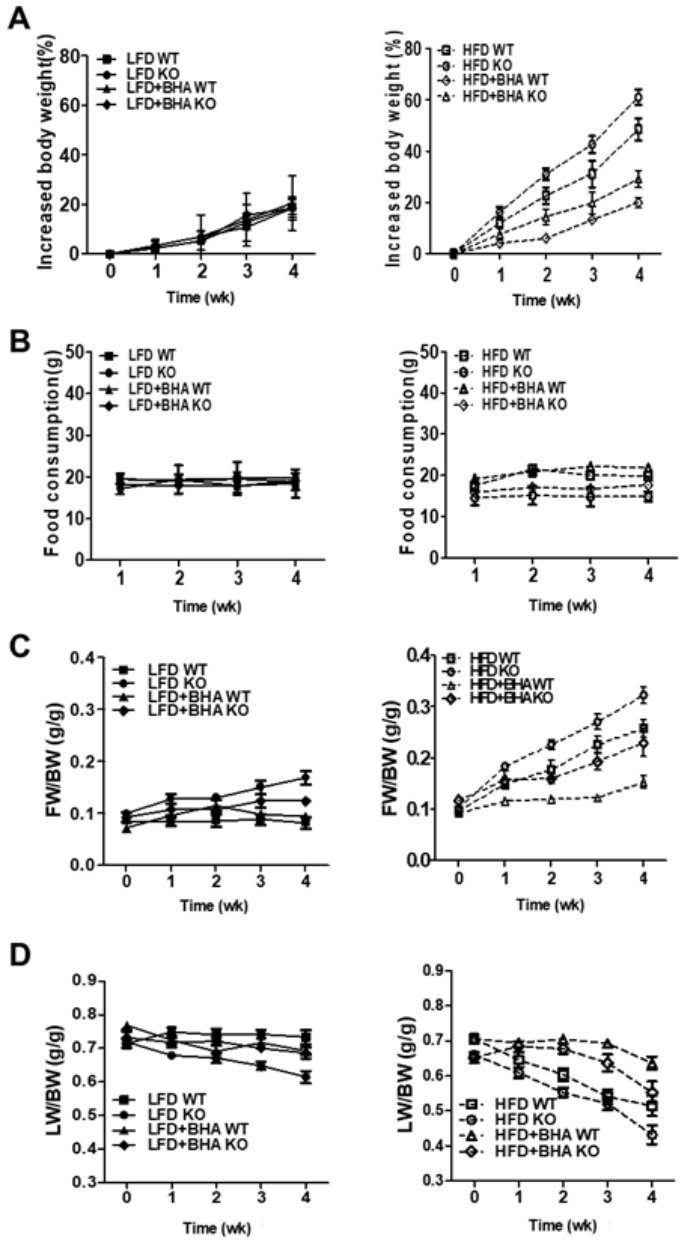

Figure 14. Body weight and body composition in response to BHA treatment in WT and IDH2 KO mice. (A) Increased body weight data of WT and IDH2 KO mice at control or BHA-treated LFD and HFD for 4 wk. (B) Food consumption in

each group over a period of 4 wk. (C&D) Fat mass and lean mass determined by NMR based on body composition of WT and IDH2 KO mice at control or BHA supplemented LFD and HFD for 4 wk. BHA: butylated hydroxyanisole.

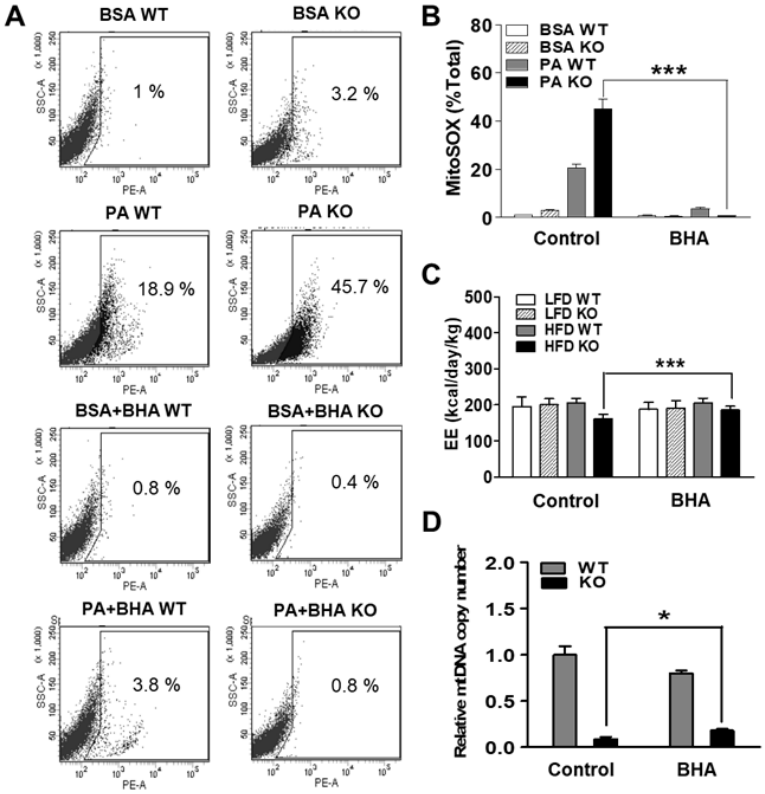

Figure 15. Effect of anti-oxidant reagent against diet-induced obesity. (A) Primary brown adipocytes from WT and IDH2 KO mice were treated with BSA or BSA-conjugated palmitate and stained with MitoSOX Red followed by FACS analysis. (B) Quantification of stained area from FACS data. (C) Energy expenditure data over 24 h period of WT and IDH2 KO mice at control or BHA supplemented LFD and HFD. (D) Relative mtDNA content expressed as a function of nDNA in BAT from control or BHA-treated HFD-IDH2 KO mice. * $p < 0.05$ and *** $p < 0.001$ vs. PA KO or HFD KO.

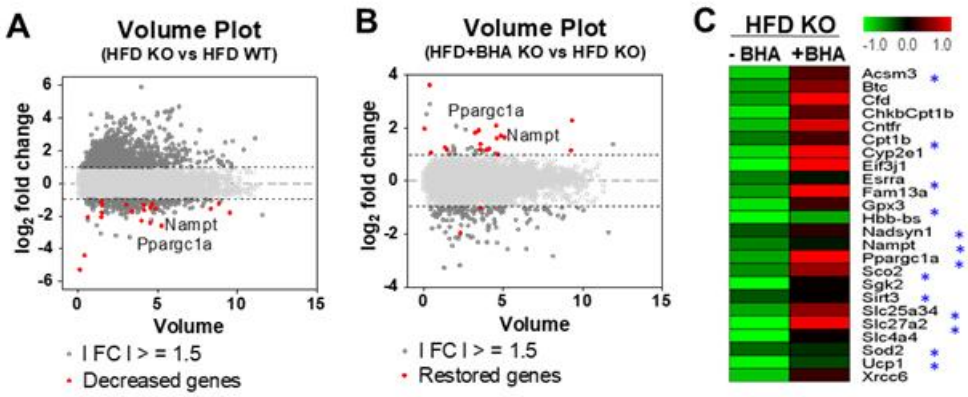

Figure 16. RNA-sequencing data by BHA in BAT of HFD-fed IDH2 KO mice. WT and IDH2 KO mice were fed with BHA-treated LFD and HFD for 4 wk. (A&B) Scatterplot of the gene expression ratio in control versus HFD WT or BHA-treated HFD-IDH2 KO mice. Fold change was cutted off by 1.5. (C) Heatmap representation of gene expression differences between control and BHA-treated HFD KO mice as determined by RNA-sequencing of BAT. Acsm3: acyl-CoA synthetase medium chain family member 3; Btc: betacellulin; Cfd: complement factor D; Cntfr: ciliary neurotrophic factor receptor; Cyp2e1: cytochrome p450 family 2 subfamily E member 1; Eif3j1: eukaryotic translation initiation factor 3; Fam13a: family with sequence similarity 13 member A; FC: fold change; Hbb-bs: hemoglobin, beta adult s chain synonyms beta s; Sco2: Sco cytochrome c oxidase assembly protein 2; Sgk2: serum/glucocorticoid regulated kinase 2; Slc25a34: solute carrier family 25 member 34; Slc27a2: solute carrier family 27 member 2; Slc4a4: solute carrier family 4 member 4; Xrcc6: x-ray repair cross complementing 6.

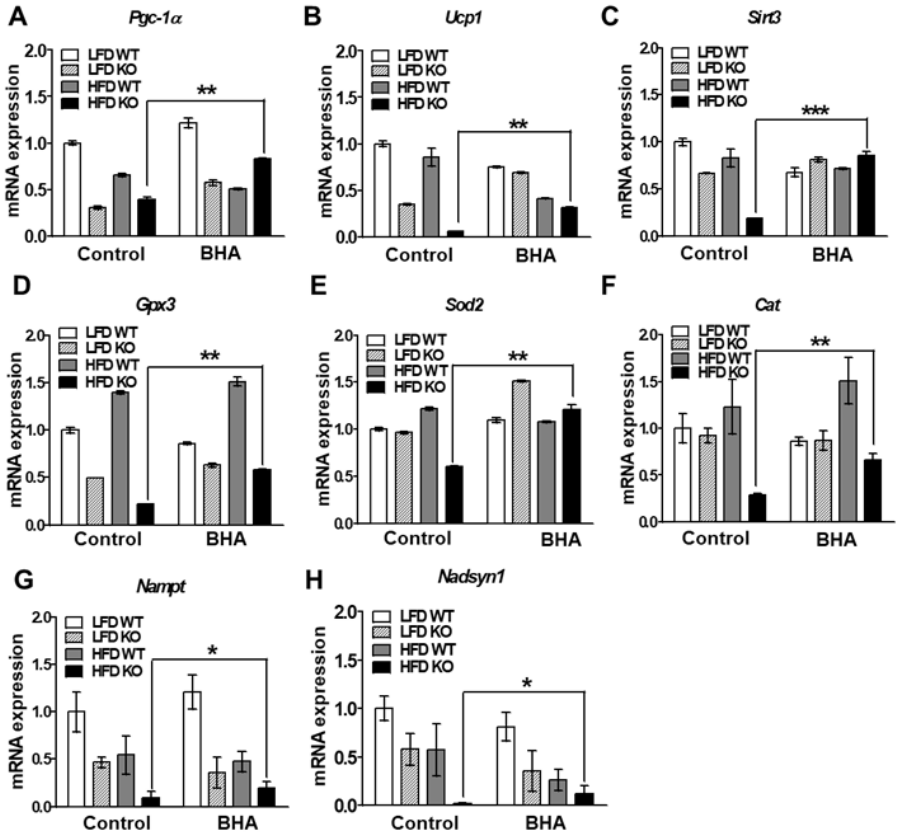

Figure 17. Anti-oxidant reagent recovers genes expression in BAT of IDH2 KO mice. Four-wk-old male WT and IDH2 KO mice were fed HFD and where indicated supplemented with BHA for 4 wk. (A-H) Genes expression levels by qPCR analysis. * $p < 0.05$, ** $p < 0.01$ and *** $p < 0.001$ vs. HFD KO.

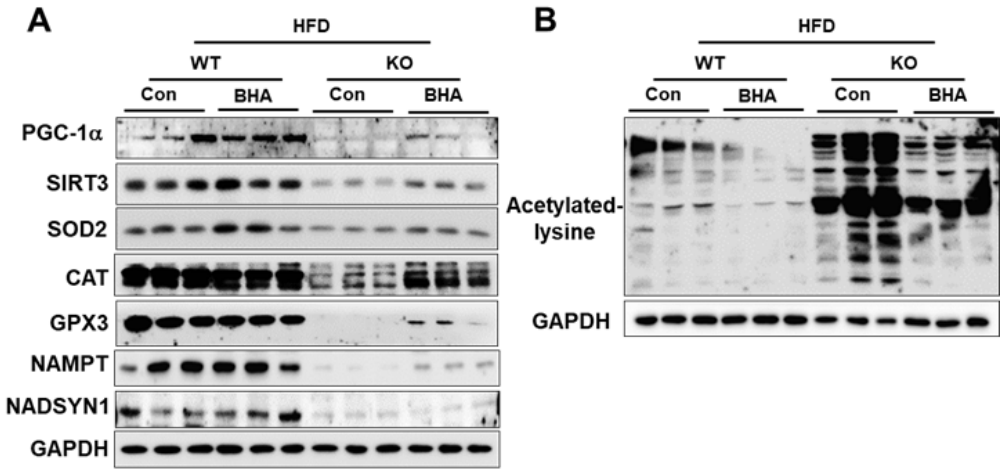

Figure 18. Anti-oxidant restores mitochondrial function in IDH2 KO mice. (A) BAT samples of WT and IDH2 KO mice were analyzed for the indicated proteins. (B) Total acetylated lysine level was measured by Western blot.

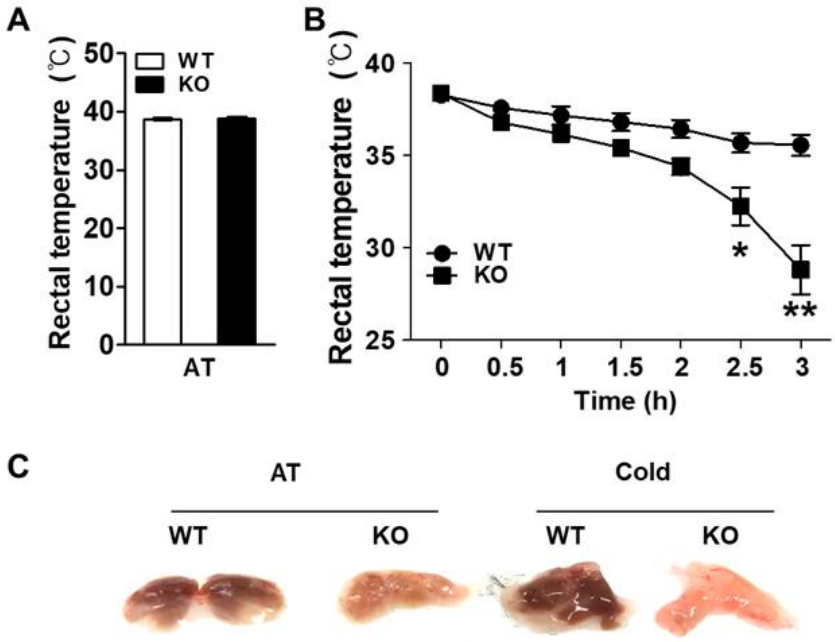

Figure 19. Measurement of body temperature in WT and IDH2 KO mice after cold exposure. (A) Basal rectal temperature of 8-wk-old WT and IDH2 KO mice measured in an ambient temperature of 25 ℃. (B) Body temperature curve of WT and IDH2 KO mice exposed to 4 ℃. (C) Representative photographs showing BAT deposits from WT and IDH2 KO mice. * $p < 0.05$ and ** $p < 0.01$ vs. WT. AT: ambient temperature

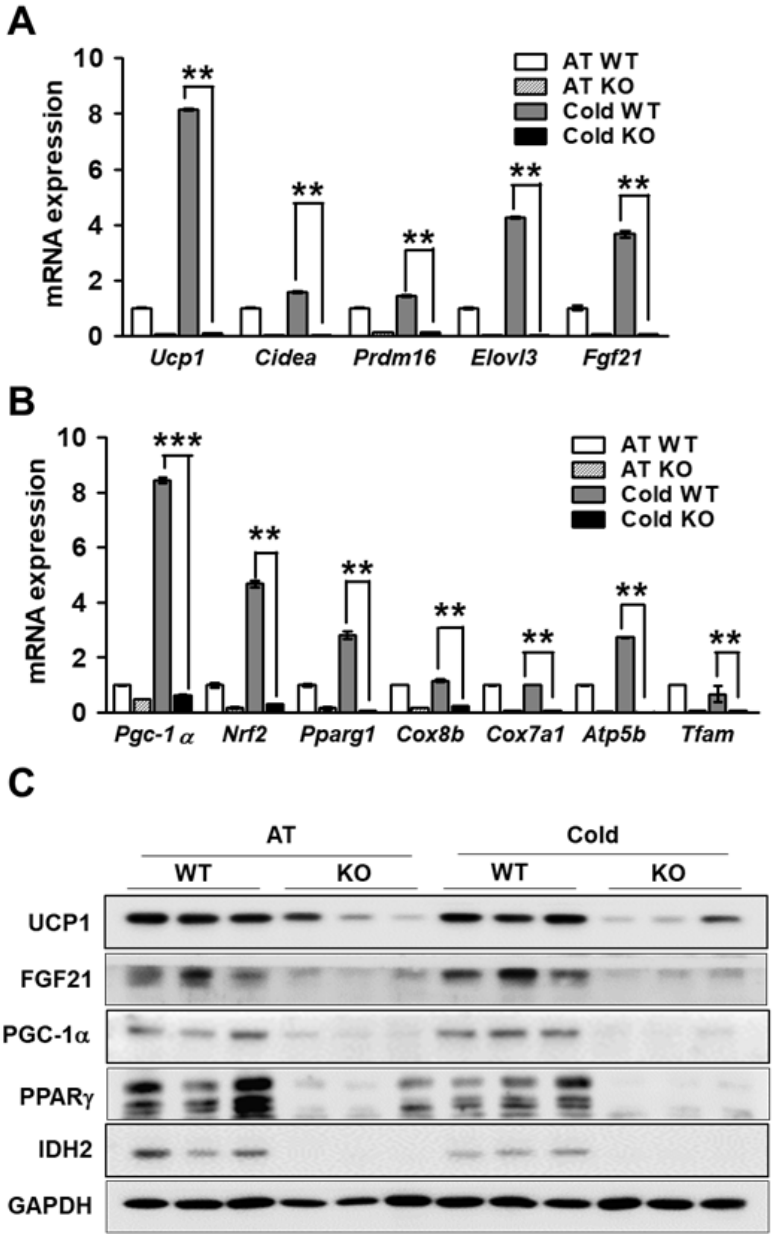

Figure 20. Thermogenic genes expression in BAT of WT and IDH2 KO mice. BAT was harvested from IDH2 KO and WT mice exposed at 25 ℃ or 4 ℃ for 3 h. The mRNA expression levels of the thermogenic marker genes (*Ucp1*, *Cidea*,

Prdm16, *Elovl3*, and *Fgf21*) (A) and mitochondrial marker genes (*Pgc-1α*, *Nrf2*, *Pparγ1*, *Cox8b*, *Cox7a1*, *Atp5b*, and *Tfam*) (B) in BAT of WT and IDH2 KO mice as determined by qPCR analysis. All genes were normalized by L32. (C) Western blot analysis of BAT from WT and IDH2 KO mice for the thermogenic and mitochondrial marker proteins. ** $p < 0.01$ and *** $p < 0.001$ vs. Cold WT. *Cox7a1*: cytochrome c oxidase subunit 7a1; *Elovl3*: elongation of very long chain fatty acids protein 3; *Fgf21*: fibroblast growth factor 21; *Nrf2*: nuclear factor erythroid 2-related factor 2; *Pparγ1*: peroxisome proliferator-activated receptor gamma 1; *Tfam*: transcription factor A mitochondrial.

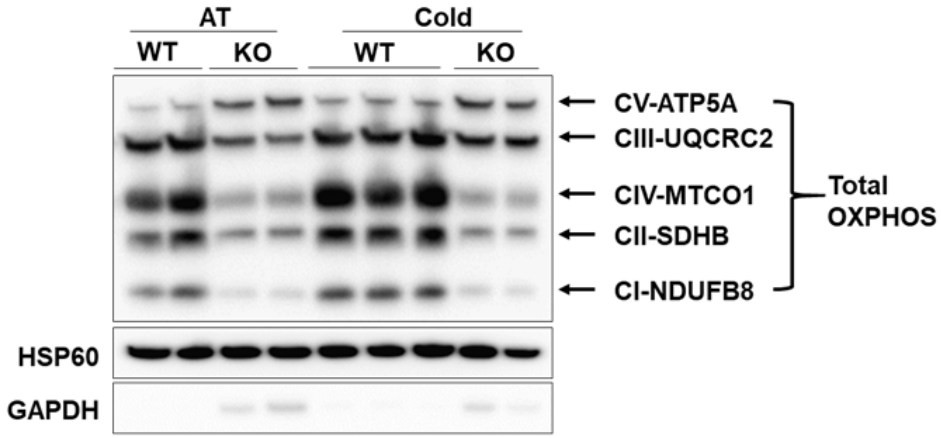

Figure 21. Mitochondrial OXPHOS levels of BAT in WT and IDH2 KO mice induced by ambient temperature or cold exposure. Levels of mitochondrial complex proteins. Western blot images of mitochondrial OXPHOS respiratory complex protein levels using the total OXPHOS antibody cocktail. HSP60 and GAPDH used as a loading control. ATP5A: ATP synthase, H^+ transporting, mitochondrial F1 complex, alpha subunit; HSP60: 60 kDa heat shock protein; MTCO1: mitochondrially encoded cytochrome c oxidase I; NDUFB8: NADH dehydrogenase (ubiquinone) 1 beta subcomplex subunit 8; OXPHOS: oxidative phosphorylation; SDHB: succinate dehydrogenase complex iron sulfur subunit B; UQCRC2: ubiquinol-cytochrome c reductase core protein 2.

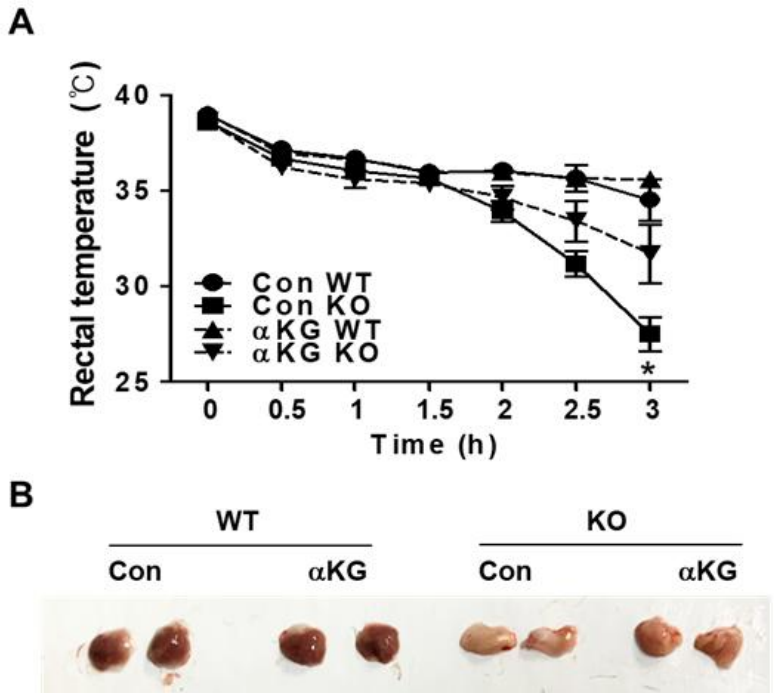

Figure 22. Recovered body temperature in IDH2 KO mice by supplement of αKG. αKG were supplemented via drinking water for 4 wk. (A) Change in rectal temperatures of WT and IDH2 KO mice after control (Con) or αKG supplementation at 4 ℃. (B) Photograph of representative BAT depots dissected from WT and IDH2 KO mice after cold exposure of control or αKG treatment. * $p < 0.05$ vs. Con KO. αKG: alpha-ketoglutarate

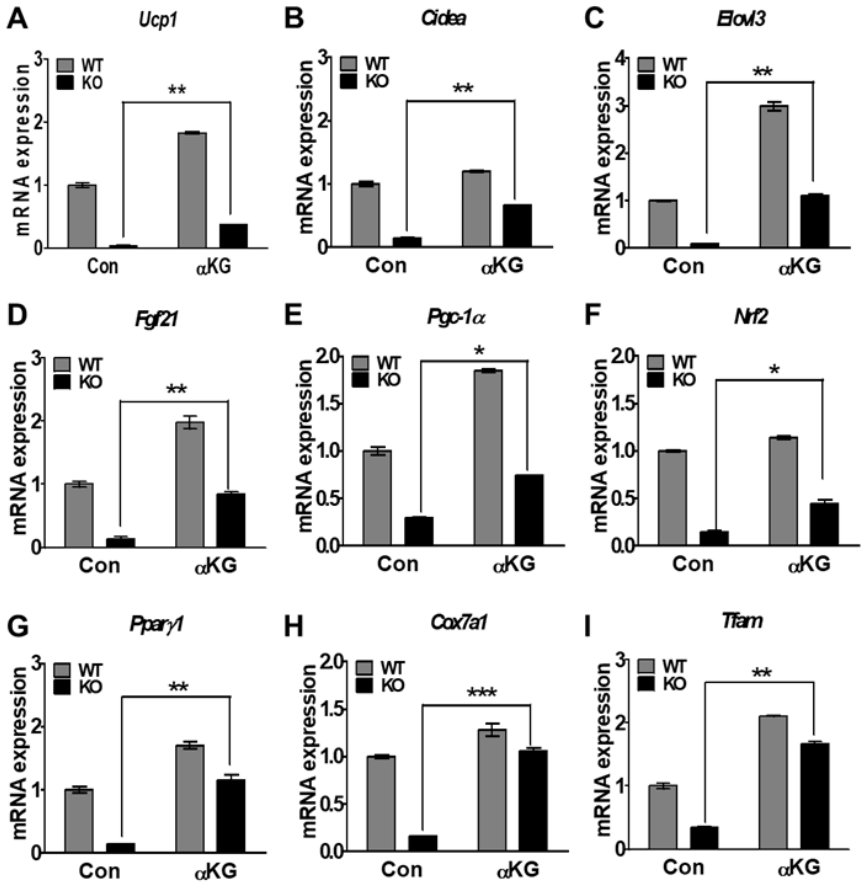

Figure 23. Genes expression by αKG in BAT of WT and IDH2 KO mice. qPCR analysis of genes expression in BAT in mice housed at cold-acclimated of control or αKG treatment. (A-I) Expression levels of *Ucp1*, *Cidea*, *Elovl3*, *Fgf21*, *Pgc-1α*, *Pparγ1*, *Cox7a1*, *Tfam*, and *Nrf2* genes were measured by qPCR. All data are shown as the mean ± SEM. * $p < 0.05$, ** $p < 0.01$ and *** $p < 0.001$ vs. Con KO.

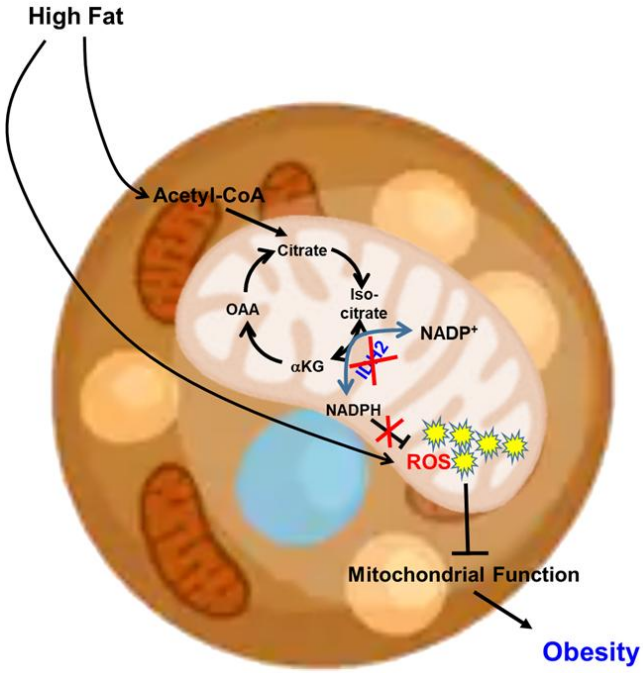

Figure 24. Scheme of IDH2-mediated effect of anti-oxidant in BAT. Deletion of IDH2 increases the metabolic stress from HFD. Subsequent rises in ROS severely reduce BAT function by overwhelming the capacity of the mitochondrial homeostasis system, increasing the oxidative stress that damages the critical mitochondrial enzyme systems. Importantly, the effects can be partially reversed by supplementation with a broadly bioavailable anti-oxidant to the diet. This supports the hypothesis that a major detrimental effect from the loss of IDH2 is accumulation of ROS. OAA: oxaloacetate.

4. Discussion

HFD-fed WT mice increase function of BAT to protect against additional weight gain from the excess caloric load (42). An inevitable metabolic effect of induced uncoupled respiration increases oxidative stress, which needs to maintain the mitochondrial homeostasis. This study found that this adaptive reaction is interrupted in IDH2 KO mice. The increase in mitochondrial activity by HFD defeats the ability of the mutant BAT mitochondria to limit the ROS accumulation. These results in acute oxidative damage to mitochondrial function involved in energy consumption and the mutant mice become obese at an increased rate relative to that observed for similarly fed WT mice.

IDH2 catalyzes the oxidative decarboxylation of isocitrate to αKG. In the mitochondria, this response is a key reversible stage of the TCA cycle. The IDH3 isoform is coupled with the capture of electrons by NAD^+ leading to the formation of NADH. On the other hand, IDH2 catalyzes a reversible reaction that utilizes $NADP^+$ and NADPH as its redox pair. Mutation in IDH2 are identified in conjunction with cancer where a mutant enzyme receives a gain-of-function to generate the oncometabolite, 2-oxoglutarate, in place of αKG (43). In contrast, the role of IDH2 in the energy metabolism of BAT remains unknown. The main physiological role for IDH2 is predicted to be in the regulation of mitochondrial $NADP^+$ and NADPH levels. Mitochondrial NADPH is critical for restricting the mitochondrial ROS accumulation. In this pathway, the critical electron capture is coupled to the thioredoxin and glutathione redox cycles.

This study demonstrates that the ablation of IDH2 results in a major mitochondrial dysfunction in the HFD-induced metabolic stress in BAT.

The levels of nicotinamide were found to have decreased in HFD-fed IDH2 KO mice and this was accompanied by reduced SIRT1 and SIRT3 levels leading to increased global acetylation of proteins. PGC-1α and SOD2 are key mitochondrial proteins that are regulated through deacetylation by SIRT1 and SIRT3 (44,45). Consistent with these data, both PGC-1α and SOD2 were found to have decreased in BAT from HFD-fed IDH2 KO mice. The reduced level of *Sod2* gene would directly result in increased ROS and the decrease in *Pgc-1α* would be coupled with the reduced expression of many other mitochondrial-related genes. Consistent with their critical role in mitochondrial gene expression, there was a serious decrease in BAT-related gene expression in a adipose tissue specific PGC-1α KO mouse model (46). This included genes such as *Sirt3* and *Sod2* which are activated by the activity of PGC-1α (47-49). The SIRT-dependent decrease in the stability of *Sod2* and *Pgc-1α* mentioned above, combined with decreased gene expression, would lead to an even greater mitochondrial dysfunction. The RNA-seq analysis, direct qPCR, and Western blot data also showed reduced expression of *Nampt* and *Nadsyn1* genes, which are required for NAD biosynthesis. This likely defines the decline in NAD^+ and $NADP^+$.

This study predicted that the excessive weight gain in HFD-fed IDH2 KO mice might be secondary to the ROS-induced damage to BAT mitochondria. Interestingly, dietary supplementation of the anti-oxidant reagent BHA limited the excess weight gain, reversed the mitochondrial dysfunction, and lowered the mitochondrial ROS in response to the loss of IDH2. Gene expressions of *Pgc-1α*, *Ucp1* and *Sirt3* accompanied by recovery of *Nampt*, *Nadsyn1* and *Sod2* genes expression. These responses provide substantial support for the proposition that the HFD-induced weight gain in IDH2 KO mice is due to the ROS-mediated mitochondrial dysfunction in BAT.

The levels of TCA cycle intermediates regulated by IDH2, such as succinate, fumarate, and malate were also lowered in IDH2 KO BAT. Interestingly, succinate increases H_2O_2 production in the presence of NAD^+-dependent substrates in complex I of the ET chain (50). For this reason, the decreased amount of succinate may indicate a partial compensatory protective system to reduce the ROS production when subjected to both IDH2 ablation and HFD. It is intriguing that even though IDH2 is not supposed to play a significant role in carbon flux under normal conditions, the reduced levels of succinate, fumarate and malate propose that IDH2 activity may take a part in TCA cycle flux. Moreover, the decreased TCA flux of citrate through succinate could also result in more citrate getting redirected to the cytoplasm for lipid biosynthesis, which could also provide to the rapid weight gain in HFD-fed IDH2 KO mice.

These data also provide evidences that IDH2 acts as a critical regulator of thermogenesis *in vivo*. IDH2 KO mice exhibited lower body temperature than WT mice after cold exposure at 4 ℃ for 3 h. This result is consistent with changed color of BAT in IDH2 KO mice and provides further demonstration that BAT function is significantly impaired in these mice after the exposure to cold. Moreover, IDH2 ablation resulted in a decrease in the expression levels of the genes involved in fat browning and mitochondrial biogenesis. These results suggest that IDH2 deficiency may contribute to declined thermogenic effect caused by mitochondrial dysfunction in BAT.

PGC-1α, the important sensor activated by a wide variety of mitochondrial biogenesis, is also the major driver of mitochondrial biogenesis and function. It promotes mitochondrial function through the interactions with NRF2 and PPARγ in various cells containing brown adipocytes (51,52). In this study, the experimental results confirmed that

expression levels of *Pgc-1α*, *Nrf2* and *Pparγ* were dramatically reduced in IDH2 KO BAT samples.

αKG is a keto acid synthesized by deamination of glutamate and is an important intermediate of the TCA cycle. It has various physiological functions including that as an anti-oxidant (53,54) or anti-cancer agent (55,56). Furthermore, αKG regulates cellular energy status through inhibiting ATP synthase and reducing oxygen consumption in mammalian and caenorhabditis elegans cells (57). Another study has shown that the supplementation of αKG enhances ten-eleven translocation activity and facilitates brown adipogenesis through αKG-mediated DNA demethylation in the *Prdm16* promoter and expression (58). Pharmacological elevation in circulating succinate drives UCP1-dependent thermogenesis by BAT *in vivo*, which stimulates robust protection against diet-induced obesity and improves glucose tolerance (59). Therefore, supplementation of intermediate metabolite may help in the recovery from thermogenic dysfunction in IDH2 KO mice. In this study, αKG supplementation dramatically recovered the body temperature upon cold exposure in IDH2 KO mice.

In summary, thsese data propose that the deficiency of IDH2 induces the HFD-mediated metabolic stress. The elevation of ROS hinders the capacity of BAT mitochondrial homeostasis, leading to a severe decrease in the BAT function. Importantly, these outcomes can be reversed by diet supplementation of a bioavailable anti-oxidant reagent with HFD. These data supports the hypothesis that the major harmful effect resulting from the ablation of IDH2 is the accumulation of ROS (Figure 24).

Although IDH2 is implicated in the regulation of energy metabolism, future studies are needed to determine the molecular mechanism, by which IDH2 regulates the energy metabolism. Thus, this study might

provide a glance into the mechanism, at least in part, for the health benefits from anti-oxidant supplementation in obese humans.

5. Summary

IDH2 regulates mitochondrial function and redox balance in multiple organs. However, the role of IDH2 is not fully elucidated in energy metabolism. BAT is the important organ for heat production and anti-obesity. This study investigated the role of IDH2 in BAT. Data showed that IDH2 KO mice challenged with HFD gained significantly more body weight than WT mice. The excess weight gains in the IDH2 KO mice were accompanied by increased levels of ROS and reduced energy expenditure in BAT. These changes were restored when the anti-oxidant BHA was supplemented to the HFD. Next, this study investigated the thermogenic activity in cold-exposed BAT. IDH2 KO mice showed a significantly reduced body temperature than WT mice after cold exposure. The ablation of IDH2 decreased thermogenic and mitochondrial biogenesis genes of BAT under cold exposure. These changes were restored by supplementation of αKG. These results provide strong *in vivo* genetic support for a role of IDH2 in energy metabolism, cold-induced thermogenesis and defense against diet-induced obesity.

References

1. Cupp JR, McAlister-Henn L: NAD^+-dependent isocitrate dehydrogenase. Cloning, nucleotide sequence, and disruption of the IDH2 gene from Saccharomyces cerevisiae. J Biol Chem 1991; 266: 22199-205.

2. Jo SH, Son MK, Koh HJ, Lee SM, Song IH, Kim YO, et al.: Control of mitochondrial redox balance and cellular defense against oxidative damage by mitochondrial $NADP^+$-dependent isocitrate dehydrogenase. J Biol Chem 2001; 276: 16168-76.

3. Al-Khallaf H: Isocitrate dehydrogenases in physiology and cancer: Biochemical and molecular insight. Cell Biosci 2017; 7: 37-55.

4. Smolkova K, Jezek P: The role of mitochondrial NADPH-dependent isocitrate dehydrogenase in cancer cells. Int J Cell Biol 2012; 2012: 273947-9.

5. Gelman SJ, Naser F, Mahieu NG, McKenzie LD, Dunn GP, Chheda MG, et al.: Consumption of NADPH for 2-HG synthesis increases pentose phosphate pathway flux and sensitizes cells to oxidative stress. Cell Rep 2018; 22: 512-22.

6. Han SJ, Choi HS, Kim JI, Park JW, Park KM: IDH2 deficiency increases the liver susceptibility to ischemia-reperfusion injury via increased mitochondrial oxidative injury. Redox Biol 2018; 14: 142-53.

7. Cao S, Liu Y, Sun W, Zhao L, Zhang L, Liu X, et al.: Genome-wide expression profiling of anoxia/reoxygenation in rat cardiomyocytes uncovers the role of mitoKATP in energy homeostasis. Oxid Med Cell Longev 2015; 2015: 756576-90.

8. Ducray F, Marie Y, Sanson M: IDH1 and IDH2 mutations in gliomas. N Engl J Med 2009; 360: 2248-9.

9. Holdhoff M, Parsons DW, Diaz LA, Jr: Mutations of IDH1 and IDH2 are not detected in brain metastases of colorectal cancer. J Neurooncol 2009; 94: 297-9.

10. Park SW, Chung NG, Han JY, Eom HS, Lee JY, Yoo NJ, et al.: Absence of IDH2 codon 172 mutation in common human cancers. Int J Cancer 2009; 125: 2485-6.

11. Lu C, Venneti S, Akalin A, Fang F, Ward PS, Dematteo RG, et al.: Induction of sarcomas by mutant IDH2. Genes Dev 2013; 27: 1986-98.

12. Kotredes KP, Razmpour R, Lutton E, Alfonso-Prieto M, Ramirez SH, Gamero AM: Characterization of cancer-associated IDH2 mutations that differ in tumorigenicity, chemosensitivity and 2-hydroxyglutarate production. Oncotarget 2019; 10: 2675-92.

13. Tommasini-Ghelfi S, Murnan K, Kouri FM, Mahajan AS, May JL, Stegh AH: Cancer-associated mutation and beyond: The emerging biology of isocitrate dehydrogenases in human disease. Sci Adv 2019; 5: 5-22.

14. Gong F, Gao L, Ding T: IDH2 protects against nonalcoholic steatohepatitis by alleviating dyslipidemia regulated by oxidative stress. Biochem Biophys Res Commun 2019; 514: 593-600.

15. Abate N: Obesity and cardiovascular disease. Pathogenetic role of the metabolic syndrome and therapeutic implications. J Diabetes Complications 2000; 14: 154-74.

16. Bell DS: The association of obesity, metabolic syndrome, diabetes, and cardiovascular disease with nonalcoholic fatty liver disease. South Med J 2009; 102: 991-2.

17. Grundy SM: Obesity, metabolic syndrome, and cardiovascular disease. J Clin Endocrinol Metab 2004; 89: 2595-600.

18. Leitner DR, Fruhbeck G, Yumuk V, Schindler K, Micic D, Woodward E, et al.: Obesity and type 2 diabetes: Two diseases with a need for combined treatment strategies. Obes Facts 2017; 10: 483-92.

19. Liu T, Li C, Shen L, Shen Y, Mao W, Li S: Heterogeneity in effects of genetically determined adiposity on insulin resistance and type 2 diabetes: The atherosclerosis risk in communities study. J Diabetes Complications 2018; 32: 330-4.

20. Park A, Kim WK, Bae KH: Distinction of white, beige and brown adipocytes derived from mesenchymal stem cells. World J Stem Cells 2014; 6: 33-42.

21. Kaisanlahti A, Glumoff T: Browning of white fat: Agents and implications for beige adipose tissue to type 2 diabetes. J Physiol Biochem 2019; 75: 1-10.

22. Bartelt A, Heeren J: Adipose tissue browning and metabolic health. Nat Rev Endocrinol 2014; 10: 24-36.

23. Sanchez-Gurmaches J, Hung CM, Guertin DA: Emerging complexities in adipocyte origins and identity. Trends Cell Biol 2016; 26: 313-26.

24. Carpentier AC, Blondin DP, Virtanen KA, Richard D, Haman F, Turcotte EE: Brown adipose tissue energy metabolism in humans. Front Endocrinol 2018; 9: 447-68.

25. Shabalina IG, Petrovic N, de Jong JM, Kalinovich AV, Cannon B, Nedergaard J: UCP1 in brite/beige adipose tissue mitochondria is functionally thermogenic. Cell Rep 2013; 5: 1196-203.

26. Kazak L, Chouchani ET, Stavrovskaya IG, Lu GZ, Jedrychowski MP, Egan DF, et al.: UCP1 deficiency causes brown fat respiratory chain depletion and sensitizes mitochondria to calcium overload-induced dysfunction. Proc Natl Acad Sci USA 2017; 114: 7981-6.

27. Song NJ, Chang SH, Li DY, Villanueva CJ, Park KW: Induction of thermogenic adipocytes: Molecular targets and thermogenic small molecules. Exp Mol Med 2017; 49: e353.

28. Van Marken Lichtenbelt W: Brown adipose tissue and the regulation

of nonshivering thermogenesis. Curr Opin Clin Nutr Metab Care 2012; 15: 547-52.

29. Thaler JP, Guyenet SJ, Dorfman MD, Wisse BE, Schwartz MW: Hypothalamic inflammation: Marker or mechanism of obesity pathogenesis? Diabetes 2013; 62: 2629-34.

30. Zhang W, Bi S: Hypothalamic regulation of brown adipose tissue thermogenesis and energy homeostasis. Front Endocrinol (Lausanne) 2015; 6: 136-45.

31. Whittle AJ, Lopez M, Vidal-Puig A: Using brown adipose tissue to treat obesity. Trends Mol Med 2011; 17: 405-11.

32. Mailloux RJ, Adjeitey CN, Xuan JY, Harper ME: Crucial yet divergent roles of mitochondrial redox state in skeletal muscle vs. brown adipose tissue energetics. FASEB J 2012; 26: 363-75.

33. Schonfeld P, Wojtczak L: Brown adipose tissue mitochondria oxidizing fatty acids generate high levels of reactive oxygen species irrespective of the uncoupling protein-1 activity state. Biochim Biophys Acta 2012; 1817: 410-8.

34. Mailloux RJ, Jin X, Willmore WG: Redox regulation of mitochondrial function with emphasis on cysteine oxidation reactions. Redox Biol 2014; 2: 123-39.

35. Park SY, Lee SM, Shin SW, Park JW: Inactivation of mitochondrial $NADP^+$-dependent isocitrate dehydrogenase by hypochlorous acid.

Free Radic Res 2008; 42: 467-73.

36. Leonardi R, Subramanian C, Jackowski S, Rock CO: Cancer-associated isocitrate dehydrogenase mutations inactivate NADPH-dependent reductive carboxylation. J Biol Chem 2012; 287: 14615-20.

37. Mogen AB, Carroll RK, James KL, Lima G, Silva D, Culver JA, et al.: Staphylococcus aureus nitric oxide synthase modulates aerobic respiratory metabolism and cell physiology. Mol Microbiol 2017; 105: 139-57.

38. Ku HJ, Ahn Y, Lee JH, Park KM, Park JW: IDH2 deficiency promotes mitochondrial dysfunction and cardiac hypertrophy in mice. Free Radic Biol Med 2015; 80: 84-92.

39. Gerhart-Hines Z, Rodgers JT, Bare O, Lerin C, Kim SH, Mostoslavsky R, et al.: Metabolic control of muscle mitochondrial function and fatty acid oxidation through SIRT1/PGC-1alpha. EMBO J 2007; 26: 1913-23.

40. Qiu X, Brown K, Hirschey MD, Verdin E, Chen D: Calorie restriction reduces oxidative stress by SIRT3-mediated SOD2 activation. Cell Metab 2010; 12: 662-7.

41. Zhang Y, Choksi S, Chen K, Pobezinskaya Y, Linnoila I, Liu ZG: ROS play a critical role in the differentiation of alternatively activated macrophages and the occurrence of tumor-associated macrophages. Cell Res 2013; 23: 898-914.

42. Chouchani ET, Kazak L, Jedrychowski MP, Lu GZ, Erickson BK, Szpyt J, et al.: Mitochondrial ROS regulate thermogenic energy expenditure and sulfenylation of UCP1. Nature 2016; 532: 112-6.

43. Gross S, Cairns RA, Minden MD, Driggers EM, Bittinger MA, Jang HG, et al.: Cancer-associated metabolite 2-hydroxyglutarate accumulates in acute myelogenous leukemia with isocitrate dehydrogenase 1 and 2 mutations. J Exp Med 2010; 207: 339-44.

44. Kumar S, Lombard DB: Mitochondrial sirtuins and their relationships with metabolic disease and cancer. Antioxid Redox Signal 2015; 22: 1060-77.

45. Cheng A, Yang Y, Zhou Y, Maharana C, Lu D, Peng W, et al.: Mitochondrial SIRT3 mediates adaptive responses of neurons to exercise and metabolic and excitatory challenges. Cell Metab 2016; 23: 128-42.

46. Uldry M, Yang W, St-Pierre J, Lin J, Seale P, Spiegelman BM: Complementary action of the PGC-1 coactivators in mitochondrial biogenesis and brown fat differentiation. Cell Metab 2006; 3: 333-41.

47. Giralt A, Hondares E, Villena JA, Ribas F, Diaz-Delfin J, Giralt M, et al.: Peroxisome proliferator-activated receptor-gamma coactivator-1alpha controls transcription of the *Sirt3* gene, an essential component of the thermogenic brown adipocyte phenotype. J Biol Chem 2011; 286: 16958-66.

48. Zhang X, Ren X, Zhang Q, Li Z, Ma S, Bao J, et al.: PGC-1α/ERRα

-Sirt3 pathway regulates daergic neuronal death by directly deacetylating SOD2 and ATP synthase β. Antioxid Redox Signal 2016; 24: 312-28.

49. Ding Y, Yang H, Wang Y, Chen J, Ji Z, Sun H: Sirtuin 3 is required for osteogenic differentiation through maintenance of PGC-1α-SOD2-mediated regulation of mitochondrial function. Int J Biol Sci 2017; 13: 254-64.

50. Zoccarato F, Cavallini L, Bortolami S, Alexandre A: Succinate modulation of H_2O_2 release at NADH: Ubiquinone oxidoreductase (Complex I) in brain mitochondria. Biochem J 2007; 406: 125-9.

51. Namani A, Li Y, Wang XJ, Tang X: Modulation of NRF2 signaling pathway by nuclear receptors: Implications for cancer. Biochim Biophys Acta 2014; 1843: 1875-85.

52. Gureev AP, Shaforostova EA, Popov VN: Regulation of mitochondrial biogenesis as a way for active longevity: Interaction between the NRF2 and PGC-1alpha signaling pathways. Front Genet 2019; 10: 435-47.

53. Lemire J, Milandu Y, Auger C, Bignucolo A, Appanna VP, Appanna VD: Histidine is a source of the antioxidant, alpha-ketoglutarate in pseudomonas fluorescens challenged by oxidative stress. FEMS Microbiol Lett 2010; 309: 170-7.

54. Long LH, Halliwell B: Artefacts in cell culture: Alpha-ketoglutarate can scavenge hydrogen peroxide generated by ascorbate and

epigallocatechin gallate in cell culture media. Biochem Biophys Res Commun 2011; 406: 20-4.

55. Tennant DA, Gottlieb E: HIF prolyl hydroxylase-3 mediates alpha-ketoglutarate-induced apoptosis and tumor suppression. J Mol Med 2010; 88: 839-49.

56. Rzeski W, Walczak K, Juszczak M, Langner E, Pozarowski P, Kandefer-Szerszen M, et al.: Alpha-ketoglutarate inhibits proliferation of colon adenocarcinoma cells in normoxic conditions. Scand J Gastroenterol 2012; 47: 565-71.

57. Chin RM, Fu X, Pai MY, Vergnes L, Hwang H, Deng G, et al.: The metabolite alpha-ketoglutarate extends lifespan by inhibiting ATP synthase and TOR. Nature 2014; 510: 397-401.

58. Yang Q, Liang X, Sun X, Zhang L, Fu X, Rogers CJ, et al.: AMPK/alpha-ketoglutarate axis dynamically mediates DNA demethylation in the *Prdm16* promoter and brown adipogenesis. Cell Metab 2016; 24: 542-54.

59. Mills EL, Pierce KA, Jedrychowski MP, Garrity R, Winther S, Vidoni S, et al.: Accumulation of succinate controls activation of adipose tissue thermogenesis. Nature 2018; 560: 102-6.

Isocitrate Dehydrogenase 2 Deficiency Induces Dysfunction of Energy Metabolism in Brown Adipose Tissue

Lee, Jae-Ho

Department of Physiology
Graduate School

Keimyung University

(Supervised by Professor Im, Seung-Soon)

(Abstract)

Isocitrate dehydrogenase 2 (IDH2) is a nicotinamide adenine dinucleotide phosphate-dependent enzyme located in the mitochondria. IDH2 also regulates mitochondrial oxidative stress by catalyzing the production of nicotinamide adenine dinucleotide hydrogen phosphate. Brown adipose tissue (BAT) is the important organ for heat production in response to cold exposure and provides a protective process against obesity. This study revealed that High fat diet (HFD)-challenged IDH2 knockout (KO) mice show increased weight gain. In addition, levels of nicotinamide were reduced in BAT of HFD-fed IDH2 KO mice and this was accompanied by increased mitochondrial dysfunction as well as decreased energy expenditure, expression of mitochondrial biogenesis

genes and reactive oxygen species scavenging. These alterations were restored when the anti-oxidant butylated hydroxyanisole was added to the diet. In addition, this study reported that IDH2 deficiency resulted in the reduction of non-shivering thermogenesis in BAT. By cold exposure, IDH2 KO mice exhibited lower body temperature and thermogenic gene expression. Interestingly, alpha-ketoglutarate supplementation improved the maintenance of body temperature and thermogenesis upon cold exposure in IDH2 KO mice. These observations demonstrated that the function of IDH2 is important for preventing obesity and increasing the heat generation in BAT.

갈색지방에서 이소시트르산 탈수소효소 2 결핍에 의한 에너지 대사의 기능 조절

이 재 호

계명대학교 대학원
의학과 생리학 전공
(지도교수 임 승 순)

(초록)

미토콘드리아 내에 있는 이소시트르산 탈수소효소 2(isocitrate dehydrogenase 2, IDH2)는 시트르산회로에서 이소시트르산을 산화적 탈탄산화시켜 α-케토글루타르산(alpha-ketoglutarate, αKG)을 생성하며, 산화적 스트레스에 대해 방어 능력을 가지고 있다고 보고되었다. 하지만 에너지 대사 조절에 있어서 IDH2의 역할은 명확하지 않다. 갈색지방은 저온 노출에 반응하여 열을 생산하여 비만에 대한 보호 기전을 제공한다. 갈색지방의 기능에 대한 분자 기전은 많이 연구되었지만, 갈색지방의 활성이 어떻게 제어되고 체내의 에너지 대사와 통합되는지 종합적으로 밝혀지지 않았다. 따라서 이번 연구는 에너지 대사에 있어서 갈색지방의 활성화에 대한 IDH2의 연관성과 그 효과를 규명하고자 하였다. 먼저 갈색지방에서 IDH2의 기능을 밝히기 위해 정상 및 IDH2 결핍 마우스를 4주간 저지방식이(10% 지방)와 고지방식이(60% 지방) 시, IDH2 결핍 마우스의 몸무게가 더 증가한 것을 볼 수 있었다.

고지방식이 후 IDH2 결핍 마우스의 갈색지방에서 니코틴아마이드 종류들의 양이 현저히 감소하였으며, 이는 미토콘드리아 기능 저하, 에너지 소비 및 항산화 작용에 관여하는 주요 유전자발현의 감소를 동반하였다. 이런 변화는 항산화제인 butylated hydroxyanisole에 의해 부분적으로 회복되었다. 다음으로 IDH2 결핍 마우스의 저온 노출 시, 마우스의 체온이 급격하게 낮아졌고 갈색지방이 백색지방과 같이 변화된 것을 확인하였다. 이와 함께 열 발생 및 미토콘드리아생성 유전자들의 발현이 감소하였고, 활성산소종의 생성이 증가하였다. 이러한 변화는 αKG를 섭취한 IDH2 결핍 마우스에서 부분적으로 회복되었다. 이러한 연구결과는 고지방식이에 의한 비만을 막기 위해 갈색지방의 기능이 중요하며, 항산화제를 통한 활성산소종의 억제가 비만을 개선할 수 있음을 확인하였다. 따라서 항산화 효능을 조절하는 IDH2가 에너지 소모를 활성화하는데 중요한 역할을 하는 것을 알 수 있다. 이러한 연구결과는 IDH2가 갈색지방조직의 기능을 활성화함으로써 열 생성 반응을 증가시킬 수 있음을 시사하며, 비만과 그와 관련한 에너지 대사성 질환의 발생을 예방하기 위한 유용한 치료 표적 중의 하나를 제시하였다는데 큰 의의가 있다고 할 수 있다.

□ 저자 약력

1986년 예천 출생
건국대학교 생명공학과 졸업
계명대학교 대학원 의학과 석사

□ 논문 및 저서

「Estrogen-related receptor γ controls sterol regulatory element-binding protein-1c expression and alcoholic fatty liver」 Biochim Biophys Acta Mol Cell Biol Lipids 2019. 8.
「SREBP-1a-stimulated lipid synthesis is required for macrophage phagocytosis downstream of TLR4-directed mTORC1」 Proc Natl Acad Sci USA 2018. 12.
「PPARαdependent Insig2a overexpression inhibits SREBP-1c processing during fasting」 Sci Rep 2017. 8.
「Metformin stimulates IGFBP-2 gene expression through PPARalpha in diabetic states」 Sci Rep 2016. 3.
「Corosolic acid ameliorates acute inflammation through inhibition of IRAK-1 phosphorylation in macrophages」 BMB Rep 2016. 5.
「Regulation of IGFBP-2 expression during fasting」 Biochem J 2015. 5.
「Melatonin ameliorates ER stress-mediated hepatic steatosis through miR-23a in the liver」 Biochem Biophys Res Commun 2015. 3.